Biogeochemistry (2019) 142:443–466
https://doi.org/10.1007/s10533-019-00546-9

Understanding how estuarine hydrology controls ammonium and other inorganic nitrogen concentrations and fluxes through the subtropical Jiulong River Estuary, S.E. China under baseflow and flood-affected conditions

Dan Yu · Nengwang Chen · Michael D. Krom · Jingjie Lin · Peng Cheng · Fengling Yu · Weidong Guo · Huasheng Hong · Xinjuan Gao

Received: 30 May 2018 / Accepted: 29 January 2019 / Published online: 8 February 2019

Abstract Higher nitrogen fluxes through estuaries increase the risk of harmful algal blooms, may expand eutrophication and can cause hypoxia within estuaries and the adjacent coastal areas. However, the key factors controlling dissolved inorganic nitrogen (DIN) concentrations and export from hydrologically dynamic and turbid estuarine systems are still poorly understood. A series of cruises with high spatial resolution under different hydrological conditions were conducted in 2015–2016 across the Jiulong River Estuary (JRE) continuum, including the estuarine turbidity maximum (ETM). During baseflow, ETMs were more intense during spring tides than neap tides due to stronger net sediment resuspension. The turbidity maxima were stronger and generally further downstream under flood-affected conditions. Based on the distribution of ammonium on the salinity gradient in the low salinity region of the estuary (< 2 PSU), we grouped all the cruises into "NH_4 Addition Pattern (AP)" and "NH_4 Removal Pattern (RP)". During baseflow, AP occurred during neap tides and RP during spring tides. An important source of ammonium to the water column was from resuspended sediments and their pore waters. Based on property-salinity plots, nitrification was likely one of the most important transformation processes in the turbid water column of the JRE, resulting in the net removal of ammonium and the net addition of nitrite. It was more intense during spring tides because there were more suspended particles carrying nitrifying bacteria. There was a major addition of DIN from estuarine processes in addition to the extra nitrogen flushed from the catchment during flood-affected flow, in particular during the first flood of the year, compared with a comparatively minor addition during baseflow. This additional DIN was likely from the breakdown products of particulate organic nitrogen accumulated

Responsible Editor: J. M. Melack.

Electronic supplementary material The online version of this article (https://doi.org/10.1007/s10533-019-00546-9) contains supplementary material, which is available to authorized users.

D. Yu · N. Chen (✉) · J. Lin · H. Hong · X. Gao
Fujian Provincial Key Laboratory for Coastal Ecology and Environmental Studies, College of the Environment and Ecology, Xiamen University, Xiamen 361102, China
e-mail: nwchen@xmu.edu.cn

N. Chen · P. Cheng · F. Yu · W. Guo · H. Hong
State Key Laboratory of Marine Environmental Science, Xiamen University, Xiamen 361102, China

M. D. Krom
Morris Kahn Marine Research Station, Department of Marine Biology, Leon H. Charney School of Marine Science, University of Haifa, 3498838 Haifa, Israel

M. D. Krom
School of Earth and Environment, University of Leeds, Leeds LS2 9JT, UK

in sediments which were then resuspended under flood-affected conditions.

Keywords Ammonium · Estuarine turbidity maximum · Hydrology · Jiulong River Estuary

Introduction

High nitrogen (N) exports from the watershed to the estuary are considered as an important process causing the degradation of the estuarine and adjacent coastal waters, including harmful algal blooms, eutrophication and even hypoxia (Mayorga et al. 2010; Paerl 1997; Seitzinger et al. 2010; Vahtera et al. 2007; Whitehead and Crossman 2012). The magnitude of different N species delivered to the coastal zone is originally determined by riverine N load subsequently modified by estuarine processes (Bianchi 2007; Erler et al. 2014; Falco et al. 2010). Estuaries, especially the estuarine turbidity maxima (ETMs), are regarded as important biogeochemical reactors for major N transformations (Abril et al. 2000; Garnier et al. 2010; Herman and Heip 1999).

As one of the major dissolved inorganic nitrogen (DIN) components in lakes, rivers, estuaries and coastal seas, ammonium can be a major pollutant from sewage wastewater and agricultural runoff. The availability of ammonium in estuaries is vital to primary production, yet too much ammonium contributes to aquatic eutrophication and its subsequent deleterious effects. Therefore, examining the biogeochemical processes involving DIN especially ammonium through the estuary is a key to understand the role of the estuary as a gatekeeper modifying N delivery to the coastal ocean.

An essential characteristic of the ETM is its sediment (particulate matter) dynamics, involving cycles of resuspension and settling of sediments at different time scales of hydrological dynamics. There are greater amount of suspended particulate materials (SPMs) during spring tides than neap tides due to enhanced resuspension in the stronger spring-tide currents (Allen et al. 1980; Grabemann et al. 1997). On an intratidal time scale, suspended particulate matter tends to deposit during slack-water periods, followed by the resuspension of easily erodible bed-source sediments during the subsequent flood or ebb periods (Grabemann et al. 1997). On a seasonal basis, the river floods, which occur during the wet season, induce strong sediment erosion in the catchment, resulting in a strong net flux of the sediments downstream and into the estuary (Park et al. 2008). Within the estuary during storms, there is additional sediment resuspension including sediments in the channel and in areas of the banks that are not subject to resuspension during the normal monthly tidal cycle of spring and neap tides.

There are strong connections between sediment dynamics and nutrient biogeochemical behavior in estuaries. Large-scale and long-periods of net deposition of particulate organic matter stimulates mineralization, resulting in a large stock of ammonium in the sediments (Middelburg et al. 1996). Sediment resuspension then causes nutrient release from the sediments to the water column (Porter et al. 2010). In addition, suspended particulate matter in the water column can modify the N chemical species as a result of the activity of bacteria attached to the particles (Abril et al. 2000). In the case of macrotidal turbid estuaries, heterotrophic bacterial activity is usually more dominant than autotrophic activity like phytoplankton assimilation in the upper turbid reaches because of low light availability (Fichez et al. 1992).

Nitrification, the oxidation of ammonium to nitrate, is an important process in the water column and sediments of many estuaries around the world (Dai et al. 2008; Damashek et al. 2016; de Wilde and de Bie 2000). The typical two-step nitrification process involves the oxidation of ammonium by ammonium-oxidizing archaea (AOA) or bacteria (AOB), followed by nitrite oxidation by nitrite-oxidizing bacteria (NOB). Both processes require free oxygen, although anoxic nitrification has been found under some unusual conditions (Bartlett et al. 2008). In the water column of turbid macrotidal estuaries, nitrification reaches the maximum in the ETM, likely because nitrifying bacteria prefer to attach to particles (Abril et al. 2000; Stehr et al. 1995). In the surface sediments of such estuaries, nitrification is also an important process, as it consumes ammonium from ammonification within the sediments and provides the majority of the available nitrate for denitrification in deeper anoxic sediments (Tobias et al. 2003). Particulate organic matter mineralization in the sediments is an important process for the increase of ammonium-N and DIN fluxes to the sea (Abril et al. 1999; Tobias

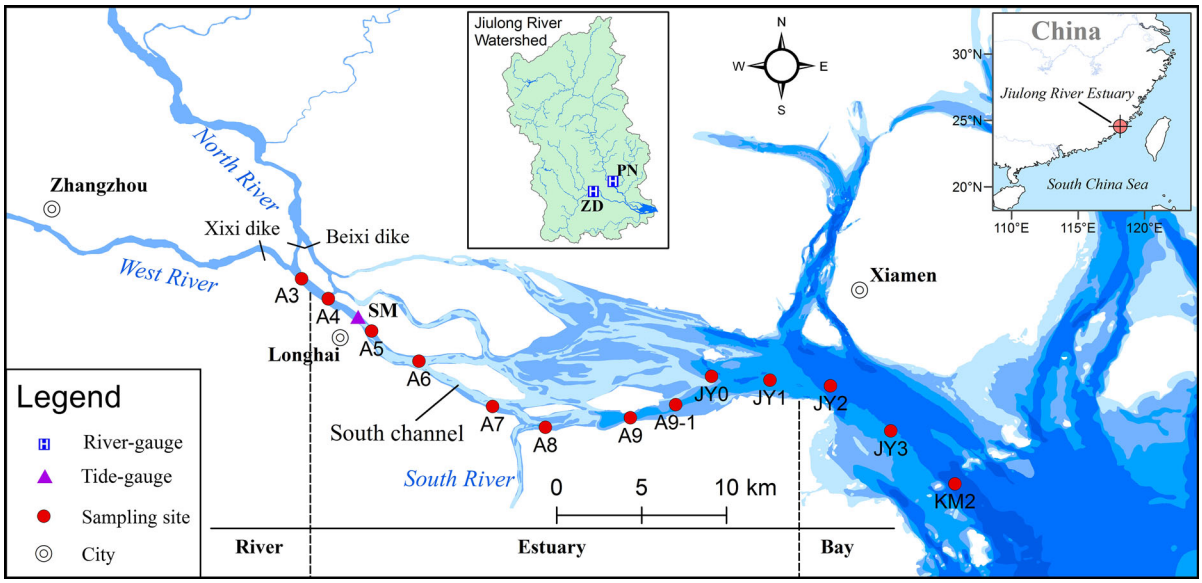

Fig. 1 Map of the Jiulong River Estuary (JRE) showing sampling sites and the tide gauge in the upper estuary marked by a triangle at Shima (SM). The different shades of blue show the average depth of water bodies. The darker blue indicates deeper water. (Color figure online)

et al. 2003), while denitrification can be a major process to remove N from the estuarine system (Crowe et al. 2012). Dissimilatory nitrate reduction to ammonium (DNRA) and anammox can also make a contribution to the turnover of N in estuary systems, though they mainly occur in anaerobic sediments (An and Gardner 2002).

As a medium-sized subtropical estuary in southeast China, the Jiulong River Estuary (JRE) is one of the earliest estuaries in which biogeochemical processes were studied in China (Li et al. 1964). Studies of nutrient dynamics in this estuary have been conducted subsequently, but most of these surveys lack data in the important low salinity areas (Chen et al. 1985; Hong and Lin 1990; Zhang et al. 1999). A recent study summarized the distribution, fluxes and decadal changes of nutrients in the JRE (Yan et al. 2012). In general, nutrients behave conservatively through the high-salinity area while nutrient cycling and behavior across the river–estuary interface (REI) is more complicated and has been less studied.

Here we conducted a series of cruises with high spatial resolution under different hydrological conditions in the JRE through the ETM to the coastal zone in 2015–2016. The specific objectives of this study were (1) to identify and characterize the ETM under different hydrological conditions (spring vs. neap tides, baseflow vs. flood-affected flow), (2) to investigate the behavior (addition and removal) of ammonium and other inorganic N species and the related biogeochemical processes in the upper JRE corresponding to different hydrological regimes of neap–spring tidal cycle, and (3) to compare how changes in the hydrological regime (baseflow vs. flood-affected flow) affect the export of DIN fluxes from the estuary to the sea.

Materials and methods

Study area

The Jiulong River is a subtropical river in southeast China, with an agriculture-dominated drainage area of 14,740 km^2 and a multi-year average rainfall of 1400–1800 mm. Two major tributaries (the North River and the West River) discharge an average annual total of 1.47×10^{10} m^3 $year^{-1}$ freshwater (two-thirds from the North River and one-third from the West River) into the JRE (Chen et al. 2018). The confluence of these two main tributaries (site A3) is described here as the river outlet (Fig. 1). A small river (the South River) converges into the middle part of the estuary. The JRE is a macrotidal estuary with an open

Table 1 Surface water environmental parameters in each cruise

Groups	Cruise dates	DO (mg L^{-1})		Temperature (°C)		pH	
		$S \leq 5$	$20 < S \leq 35$	$S \leq 5$	$20 < S \leq 35$	$S \leq 5$	$20 < S \leq 35$
NH_4-N addition pattern	2015/5/6	3.55 ± 0.35	7.51 ± 0.65	24.8 ± 0.2	22.9 ± 0.3	7.25 ± 0.21	8.02 ± 0.11
	2015/7/14	4.32 ± 0.33	5.87 ± 0.32	29.7 ± 0.1	27.8 ± 0.4	7.32 ± 0.04	8.12 ± 0.04
	2016/5/14	6.12 ± 0.35	6.93 ± 0.33	25.3 ± 0.8	24.4 ± 0.7	6.94 ± 0.17	8.00 ± 0.06
	2016/12/23	7.13 ± 0.37	9.10 ± 0.13	19.5 ± 0.4	18.1 ± 0.2	6.89 ± 0.23	8.02 ± 0.05
	Subtotal	5.28 ± 1.64	7.41 ± 1.26	24.4 ± 4.3	23.7 ± 4.1	7.10 ± 0.22	8.06 ± 0.05
NH_4-N removal pattern	2015/4/19	2.93 ± 0.17	8.34 ± 1.02	23.4 ± 0.1	21.1 ± 0.7	7.37 ± 0.09	8.00 ± 0.13
	2015/10/17	6.28 ± 0.37	6.93 ± 0.60	24.7 ± 0.3	25.0 ± 0.2	7.28 ± 0.16	8.17 ± 0.07
	2015/11/25	4.51 ± 1.32	7.72 ± 0.50	24.2 ± 0.6	23.3 ± 0.9	7.00 ± 0.08	7.94 ± 0.17
	2016/7/7	5.53 ± 0.43	6.95 ± 0.26	29.6 ± 0.3	29.5 ± 0.3	7.08 ± 0.09	7.98 ± 0.13
	2016/7/25	3.81 ± 0.08	5.15 ± 0.27	31.5 ± 0.2	30.3 ± 0.4	7.19 ± 0.02	8.06 ± 0.12
	2016/9/24	6.67 ± 0.94	6.98 ± 0.10	28.6 ± 0.1	27.3 ± 0.2	7.19 ± 0.26	7.87 ± 0.05
	Subtotal	4.95 ± 1.58	7.01 ± 1.07	27.0 ± 3.3	26.1 ± 3.6	7.18 ± 0.14	8.00 ± 0.10

Data indicate as mean ± standard error. There are no significant differences between the groups of NH_4 Addition Pattern and NH_4 Removal Pattern in each parameter in a same salinity group ($p > 0.05$). NH_4-N Addition Pattern indicates that an ammonium addition pattern was observed in the upper estuary. NH_4-N Removal Pattern indicates that an ammonium removal was observed in the upper estuary

S salinity (PSU)

water area of about 100 km^2 and a depth of 3–16 m. River water flows into the Xiamen Bay mainly through the south channel of the estuary (Guo et al. 2005). The average tidal range is 3.9 m, while the maximum tidal range is 6.4 m (Jiang and Wai 2005). Water temperature ranges from 13 to 32 °C (Yang and Hu 1996). The average flushing time of the JRE is about 2–3 days during baseflow (Cao et al. 2005). Along the river bank in the middle estuary, there are small-scale areas of mangroves which are dominated by *Kandelia obovate* (Chen et al. 2016).

Sampling and laboratory analysis

A total of ten cruises in the JRE were conducted from May 2015 to December 2016. As the JRE was vertically well mixed most of the time because of the relatively shallow depth and large tidal amplitude, we mainly collected surface waters from a series of stations (A3–KM2). A limited number of bottom water samples (A5–A8) were collected in the upper estuary to check the mixing (Fig. 1). In addition, to acquire a high-resolution observation at the river-estuary interface (REI), a number of additional surface water samples were collected between the main selected stations to add higher resolution within the salinity range of 0–5 PSU. A series of water quality parameters (salinity, DO, pH, temperature) were measured by a portable water quality 161 Meter (WTW Multi 3430, Germany) on deck (Table 1). CTD casts were performed at fixed stations on 6th May 2015 (close to a neap tide) and 25th November 2015 (close to a spring tide) to examine the stratification of the estuary. The calibration of the WTW and CTD sensors were made before cruises, with pH buffers and calibration standards. All water samples were filtered through GF/F (0.7 μm) Whatman glass microfibre filters on the ship. All the filtered water samples and particulate samples were stored in a cool container on the ship before delivery to the laboratory at Xiamen University.

All water samples were stored at 4 °C before analysis of dissolved nutrients and were determined within less than 48 h. Filters were frozen at − 20 °C before analysis of SPM. All SPM weights were determined as the differences between the unfiltered and filtered GF/F membranes after oven-drying (105 °C) to constant weights. Filtered water was analyzed by a SEAL AutoAnalyzer 3 for concentrations of nitrate-N (NO_3-N), nitrite-N (NO_2-N) and ammonium-N (NH_4-N). The instrument detection limit was 0.1 μmol L^{-1} for NO_3-N, 0.04 μmol L^{-1}

for NO_2-N, and 0.5 μmol L^{-1} for NH_4-N. DIN was summed from NO_3-N, NO_2-N, and NH_4-N. The precision of each nutrient form was estimated by repeated determinations of 10% of the samples and the relative error was 3–5%. For the quality control in the laboratory, a standard reference material provided by China State EPA was used to check the instrument performance, which was within − 1 to + 4% from the standard concentration.

In order to examine the potential ammonium oxidation rates and nitrite oxidation rates in the upper and lower estuary, surface water samples at station A8 and JY3 were collected during the cruise on 23rd December 2016 and incubated using an inhibitor technique applicable to coastal marine environments (Bianchi et al. 1997; Dai et al. 2008). 5 L water samples were homogenized in a pre-cleaned and water sample rinsed container, and then 250 mL water samples were measured into three sets of 300 mL brown glass bottles (duplicate in each set). In one set of the bottles, allylthiourea (ATU, final concentration at 100 mg L^{-1}) was added to inhibit the oxidation of ammonium to nitrite; while in another set $NaClO_3$ (final concentration at 10 mg L^{-1}) was added to inhibit the oxidation of nitrite to nitrate; a third set was run with no addition of an inhibitor to act as a control. All the bottles were loosely capped and incubated on a shaker in the lab at a constant temperature, to avoid settling of particles and deficiency of oxygen. Less than 10 mL of sub-samples were taken at the time 0 h, 24 h, 48 h, 72 h. Sub-samples were then filtered by 0.45 μm CA membrane and stored at 4 °C before the measurement of NO_3-N, NO_2-N, and NH_4-N. The decrease of NO_2-N concentration over incubation time in the set with ATU inhibitor was used to estimate the potential nitrite oxidation rates and the increase of NO_2-N in the set with $NaClO_3$ was used to estimate the potential ammonium oxidation rates.

Auxiliary data collection and data analysis

Daily rainfall records for seven weather stations in the catchment were obtained from Weather China (http://www.weather.com.cn/). Hourly river discharge was obtained from hydrological stations (PN in the North River and ZD in the West River). The river discharge recorded at hydrological stations (PN and ZD) was extrapolated to the river mouth using the ratios of the drainage area between them. Data of tidal height monitored at Shima (SM, in the upper JRE; Fig. 1) were available from National Marine Data and Information Service (http://www.coi.gov.cn/).

To quantify the amount of nutrients reaching the coastal zone, the nutrient fluxes across the REI and estuary–coast interface (ECI) were calculated. The REI flux (t day^{-1}) was calculated by multiplying the concentration of the most downstream freshwater site (salinity < 0.1 PSU) and the river water flow (m^3 day^{-1}) on the sampling day. The ECI flux (t day^{-1}) represents the nutrient export from the lower estuary to coastal water at the interface with salinity = 30 PSU and was calculated using the procedure developed by Officer (1979). A best regression line fit was made to the observed concentration and salinity values in the high salinity region in the lower reaches of the estuary (typically conservative mixing). This regression line was then extrapolated back to salinity = 0 PSU to get a calculated concentration value, C_0^*. ECI fluxes were then obtained by multiplying the total river water flow (m^3 day^{-1}) on the sampling day and C_0^*. The observed concentration of nutrients from the most downriver freshwater sample was defined as C_0. The changes of N fluxes between REI and ECI were used to quantify the amount of addition or removal of each DIN species. To acquire more quantitative analysis, we also calculated the N deviations (denoted as N offset) from the conservative lines for the low salinity points. Positive N offset indicates N addition in the low salinity area and negative N offset indicates N removal.

Nutrient biogeochemical behaviour across the river–estuary–coast continuum was explored by plotting concentration against salinity. To better identify the factors controlling the ammonium behaviours, we divided the cruises into two groups–the NH_4 Addition Pattern (AP) and NH_4 Removal Pattern (RP) according to the characteristics of ammonium-N-Salinity diagrams in the low salinity region.

In this study, we defined the 'baseflow' hydrological condition as the period when the river discharge was less than 1.2 times of the previous baseflow, which was estimated using an automatic segmentation procedure (BFI {F}: Smoothed Minima method) (Nathan and McMahon 1990). By contrast, the period when the discharge was more than 1.2 times of the previous flow was defined as flood-affected

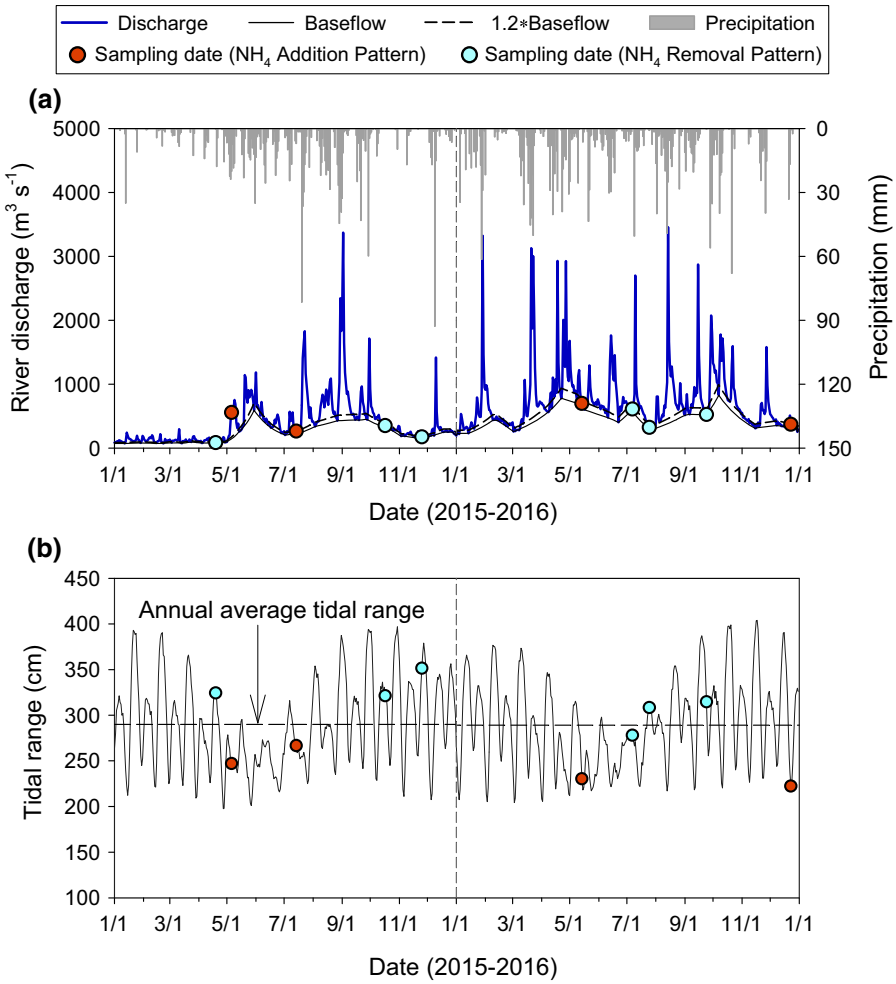

Fig. 2 **a** Daily river discharge and precipitation in the Jiulong River watershed in 2015–2016 and **b** Daily tidal range recorded at Shima (SM) in the upper Jiulong River Estuary in 2015–2016. Red circles show the sampling date of cruises in which an ammonium addition pattern was observed in the upper estuary and blue circles show sampling when an ammonium removal pattern was observed. (Color figure online)

conditions, according to the definition used in our previous research in the JRE system (Chen et al. 2018; Gao et al. 2018).

Results

Meteorological and hydrological conditions in 2015–2016

The total rainfall in 2015 was 1754 mm, of which 82% occurred in the wet season from April to October (Fig. 2a). This is a typical distribution of precipitation in the area which is affected by the Asian monsoon system and by occasional typhoons from May to November (Ren et al. 2001). The total rainfall in 2016 was 2314 mm, considerably higher than that in 2015, as a series of rainfall events occurred in the period from early January 2016 until late November 2016 (Fig. 2a). Those 2 years, particularly the year of 2016, were among the wetter years with relatively abundant rains, compared to the multi-year average rainfall of 1400–1800 mm.

River discharges were low (73 $m^3\ s^{-1}$ to 297 $m^3\ s^{-1}$) from January to April in 2015 and then started to rise in late April (Fig. 2a). The cruise in May 2015 was carried out during the rising limb of the hydrography of the first flood event of the year, which was regarded as under the flood-affected condition (Fig. 2a). River discharges ranged from 84 $m^3\ s^{-1}$ (April 2015) to 697 $m^3\ s^{-1}$ (May 2015). All the cruises except May 2015 were carried out under baseflow conditions. In general, 2016 was relatively wetter with a water yield (discharge/drainage area) of 1.5 m $year^{-1}$ than the year of 2015 with 0.82 m $year^{-1}$ water yield. These water yields

corresponded to 47% of the rainfall in 2015 and 65% in 2016.

Daily tidal ranges (the vertical difference between the high tide and the succeeding low tide) in the JRE in 2015–2016 are shown in Fig. 2b. Annual tidal range at the Shima tidal gauge (SM, in the upper JRE) was 290 cm in 2015 and 289 cm in 2016, respectively. Tidal ranges in cruises with the NH_4 AP were 241 cm on average with a standard error (SE) of 19 cm, which was significantly lower than the mean (± SE) value of 316 (± 24) cm in the NH_4 RP ($p < 0.01$).

Water environmental parameters

Average DO concentration, temperature and pH in the surface water of the low and high salinity ranges are listed in Table 1. The lowest DO concentration was about 2.5 mg L^{-1}, which was higher than the accepted upper limit for hypoxia (DO < 2 mg L^{-1}). DO in the high salinity area was about 2 mg L^{-1} higher than that in the low salinity area on average. Water temperature in the group of NH_4 AP ranged from 17.9 to 30.0 °C (24 °C on average), with the lowest value on 23rd December 2016 and the highest value on 14th July 2015, while the temperature ranged from 20.1 to 31.7 °C (26 °C in average) in the group of NH_4 RP. There were no significant differences in water temperature between the two groups ($p > 0.05$).

The vertical salinity and temperature profile along the JRE is shown in Fig. 3. The JRE can be classified as a partially stratified estuary, as there was some stratification during neap tides, particularly in the middle and lower part of the estuary. During the cruise on 6th May 2015 (close to a neap tide), the top-to-bottom salinity stratification of the JRE was less than 0.5 PSU in the upper estuary (< 6 km) and less than 3 PSU in the lower estuary (< 13 km), while it could exceed 5 PSU in the middle (6–13 km) and in the lower part of the estuary (20–30 km). There was less than 2 PSU of top-to-bottom stratification through the whole estuary during the cruise on 25th November 2015 (close to a spring tide). The vertical temperature stratification was less than 1 °C during both cruises. The largest vertical water density difference (> 5 kg m^3) occurred in the lower part of the estuary during the neap tide examples (Fig. 3e). DO at the bottom was 0.48–1.19 mg L^{-1} lower than that at the surface in the low salinity area (< 2 PSU), but it was higher than the surface layer (> 7 PSU at A8 on 23rd December 2016) where there was a large vertical salinity gradient and the water density difference was 5.82 kg m^3 (Table 2).

Variations of suspended particulate materials

There were significantly higher SPM during spring tides in the group of NH_4 RP (104 ± 78 mg L^{-1} as mean ± SE) than during neap tides in the group of NH_4 AP (54 ± 29 mg L^{-1}) ($p < 0.01$) (Fig. 4). Maximum SPM ranged from 62 to 97 mg L^{-1} in the AP group during baseflow, while it varied from 142 to 363 mg L^{-1} in RP group during baseflow. Maximum SPM was 104 mg L^{-1} in the flood-affected cruise in May 2015 (Fig. 4). In most cruises, maximum SPM was observed at the salinity around 0.3–1.2 PSU in both groups, except the cruise on 19th April 2015 and 7th July 2016, when it was observed at 16.5 PSU and 8.9 PSU, respectively (Fig. 5a, b).

The relationship between nitrogen concentrations and salinity

Inorganic nitrogen concentrations of the surface and bottom water samples against salinity during two cruises (during a neap tide and a spring tide) are shown in Fig. 5. Data points of bottom water still followed the pattern formed by surface water samples, even during the cruise close to a neap tide when there was some salinity stratification (salinity differences of 1–7 PSU) in the middle part of the estuary. Therefore, data of surface and bottom water were combined in the following results interpretation.

During most cruises, the data were positioned above or below the conservative mixing line, indicating the addition or removal of DIN within the estuary (Fig. 6). During baseflow conditions in cruises with the NH_4 AP, NH_4-N gradually increased within the salinity range of 0–2 PSU and then decreased linearly against salinity in all cruises (Fig. 6c). Taking the addition in December 2016 for an example, NH_4-N reached 85.8 μmol L^{-1} at the salinity of 1.6 PSU, while there was only 72.0 μmol L^{-1} at salinity = 0 PSU. During baseflow in NH_4 RP, NH_4-N decreased in the salinity range of 0–2 PSU, followed by linearly decreasing with increasing salinity (Fig. 6d). In November 2015, NH_4-N dropped from 58.9 to 46.3 μmol L^{-1} at a rate of 8.4 μmol L^{-1} per salinity unit in the salinity range of 0.4–1.9 PSU, and then

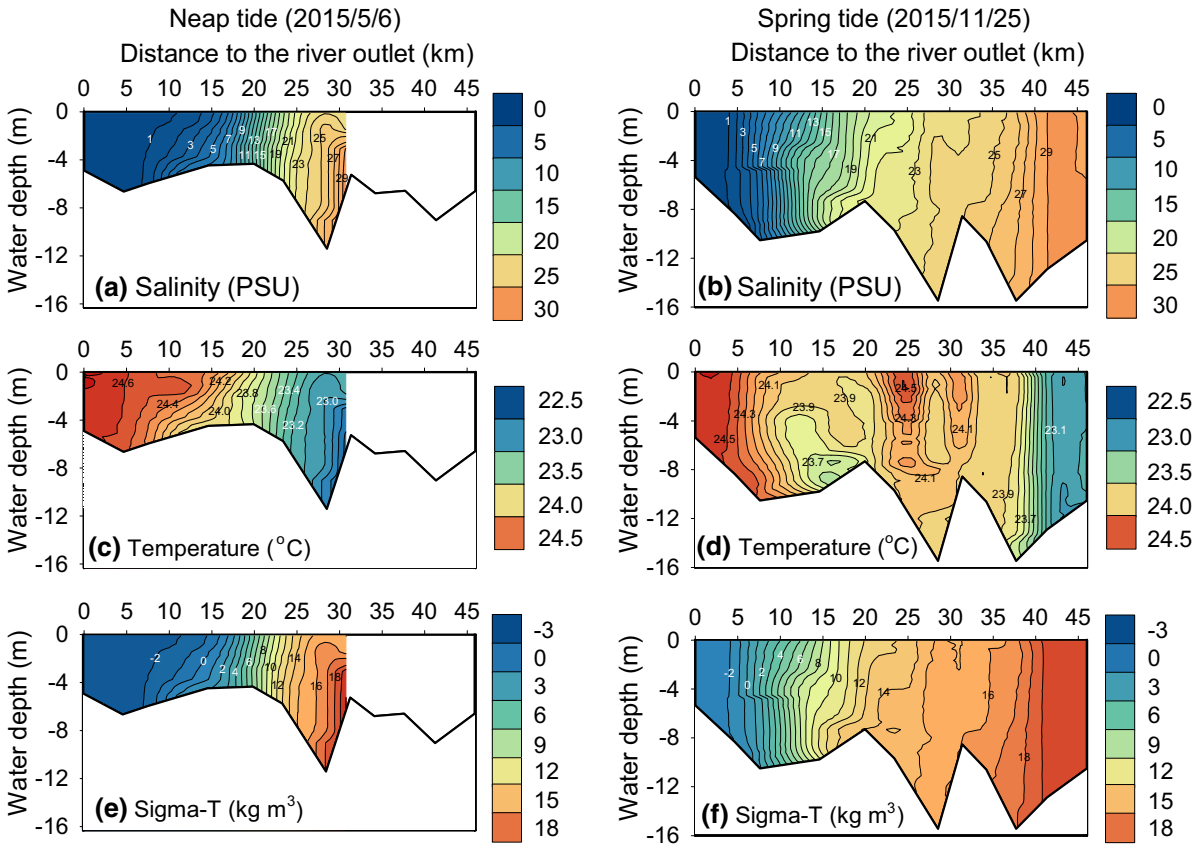

Fig. 3 Vertical salinity, temperature and water density (Sigma-T) profile along the Jiulong River–Estuary–Bay during the cruises on 6th May 2015 close to a neap tide (in NH_4-N Addition Pattern group) and 25th November 2015 close to a spring tide (in NH_4-N Removal Pattern group). Data were not available for the bay on 6th May 2015. NH_4-N Addition Pattern indicates that an ammonium addition pattern was observed in the upper estuary. NH_4-N Removal Pattern indicates that ammonium removal was observed in the upper estuary

decreased linearly by 0.8 μmol L^{-1} per salinity unit. In the flood-affected cruise in May 2015, NH_4-N increased from 129.1 μmol L^{-1} at salinity = 0 PSU to a maximum of 150.4 μmol L^{-1} at the salinity of 0.9 PSU (Fig. 6c).

The NO_2-N behavior exhibited similar trends in every cruise (Fig. 6e, f). Peak NO_2-N concentrations were always observed downstream of the ETM at around the salinity of 3–5 PSU. NO_2-N increments (in the salinity of 0–5 PSU) in May 2016 and December 2016 were less than 2.8 μmol L^{-1} during baseflow in the AP, while the highest increment was 20 μmol L^{-1} in October 2015 during baseflow in the RP.

NO_3-N almost followed the conservative mixing line (a linear line starts from the zero salinity point and ends at the highest salinity point) in most cruises, except a small change at around the salinity of 2–7 PSU in May 2016 and a small increase at the salinity < 2 PSU in December 2016 (Fig. 6g, h).

Ammonium oxidation rates and nitrite oxidation rates from incubation experiments

As shown in Table 3, nitrification rates (ammonium oxidation and nitrite oxidation) in the lower salinity area were about 13 times that in the high salinity area. At the salinity of 2.1 PSU, ammonium oxidation rate was 8.78 μmol N L^{-1} day^{-1}, around 10 times faster than that of 0.82 μmol N L^{-1} day^{-1} of nitrite oxidation rate.

Table 2 Environmental parameters of surface and bottom water during the cruises on 6th May 2015 and 23rd December 2016 (close to neap tides in NH_4 Addition Pattern group), and on 25th November 2015 and 7th July 2016 (close to spring tides in NH_4 Removal Pattern group)

Cruise dates	Sample stations	Water layers	Salinity (PSU)	Temperature (°C)	Density (kg m^3)	Sigma-T (kg m^3)	DO (mg L^{-1})
2015/5/6 (Neap tide)	A5	Surface	0.6	24.5	997.7	− 2.3	3.24
		Bottom	1.0	24.4	998.0	− 2.0	N/A
	A6	Surface	1.8	24.4	998.5	− 1.5	3.96
		Bottom	7.0	23.9	1002.6	2.6	N/A
	A7	Surface	7.0	24.0	1002.6	2.6	3.15
		Bottom	9.5	23.9	1004.5	4.5	N/A
	A8	Surface	14.0	23.7	1007.9	7.9	4.49
		Bottom	15.9	23.6	1009.4	9.4	N/A
	JY0	Surface	23.5	23.2	1015.2	15.2	7.01
		Bottom	29.8	22.6	1020.1	20.1	N/A
2016/12/23 (Neap tide)	A5	Surface	0.0	18.8	998.4	− 1.6	7.96
		Bottom	0.0	18.8	998.4	− 1.6	7.48
	A6	Surface	0.0	19.4	998.3	− 1.7	7.18
		Bottom	0.0	19.3	998.3	− 1.7	7.37
	A7	Surface	0.3	19.7	998.5	− 1.5	6.69
		Bottom	2.6	19.0	1000.4	0.4	N/A
	A8	Surface	2.1	20.2	999.8	− 0.2	6.68
		Bottom	9.5	19.2	1005.6	5.6	7.21
	JY3	Surface	24.2	18.1	1017.0	17.0	9.17
		Bottom	24.9	17.9	1017.6	17.6	9.19
2015/11/25 (Spring tide)	A3	Surface	0.4	24.6	997.5	− 2.6	2.73
		Bottom	0.4	24.6	997.5	− 2.6	N/A
	A4	Surface	1.2	23	998.5	− 1.6	6.43
		Bottom	1.2	24.5	998.1	− 1.9	5.24
	A5	Surface	4.1	24.2	1000.3	0.3	3.36
		Bottom	4.7	24.7	1000.7	0.7	N/A
	A7	Surface	16.3	24.3	1009.5	9.5	6.37
		Bottom	19.5	24.9	1011.7	11.7	7.50
	JY3	Surface	28.8	22.3	1019.4	19.4	8.34
		Bottom	28.7	22.4	1019.3	19.3	8.24
2016/7/7 (Spring tide)	A6	Surface	0.4	29.6	996.1	− 3.9	5.74
		Bottom	0.4	29.7	996.0	− 4.0	5.39
	A7	Surface	3.3	29.8	998.2	− 1.8	5.15
		Bottom	3.2	30.0	998.0	− 2.0	4.98
	A8	Surface	8.9	29.9	1002.3	2.3	6.68
		Bottom	9.0	29.7	1002.4	2.4	7.21

NH_4-N Addition Pattern indicates that an ammonium addition pattern was observed in the upper estuary. NH_4-N Removal Pattern indicates that an ammonium removal was observed in the upper estuary

N/A not available

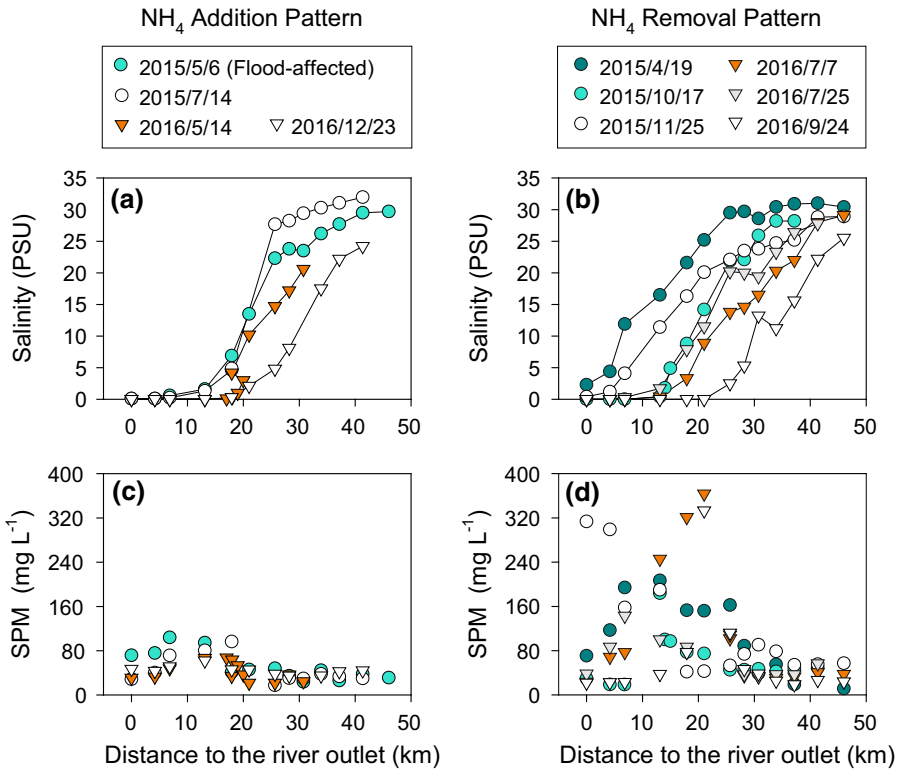

Fig. 4 Spatial variations of salinity and suspended particulate matter (SPM) along the Jiulong River–Estuary–Bay gradient in 2015 (circles) and 2016 (triangles). NH_4-N Addition Pattern indicates that an ammonium addition pattern was observed in the upper estuary. NH_4-N Removal Pattern indicates that an ammonium removal was observed in the upper estuary. The river outlet is defined as the confluence (site A3) of the North River and West River (each point refers to a corresponding site presented in Fig. 1)

Inorganic nitrogen exports through the Jiulong River Estuary

The linear regression equations and R^2 in high salinity area obtained from the procedure developed by Officer (1979) are listed in Table 4. Here we defined ΔC_0 as the difference between the calculated river (salinity = 0 PSU) concentration (C_0^*) and the observed concentration (C_0) at the location in the river closest to JRE. ΔC_0 of NH_4-N was positive (0.3–7.0 μmol L^{-1}), indicating higher calculated NH_4-N (C_0^*) than the observed NH_4-N (C_0), in the group of NH_4 AP under baseflow conditions. The largest ΔC_0 of NH_4-N (71.5 μmol L^{-1}) was found during the flood-affected cruise in May 2015. ΔC_0 of NH_4-N was negative (− 3.0 to − 20.6 μmol L^{-1}), showing lower calculated NH_4-N C_0^* than observed NH_4-N (C_0), in the NH_4 RP group. For NO_3-N, ΔC_0 was from − 4.1 to 19.2 μmol L^{-1} in the AP and from − 14.9 to 7.4 μmol L^{-1} in the RP. During baseflow, ΔC_0 of NO_2-N was 4.0–14.4 μmol L^{-1} in the AP, while there was a larger increase of ΔC_0 (16.5–25.8 μmol L^{-1}) in the RP. ΔC_0 of NO_2-N was 25.8 μmol L^{-1} during the flood-affected cruise in May 2015. In general, ΔC_0 of NH_4-N and NO_2-N showed significant differences between the AP and RP under baseflow conditions (p = 0.017 for NH_4-N and p = 0.011 for NO_2-N), while there was no significant difference in ΔC_0 of NO_3-N (p = 0.120) (Table 4).

To quantify the addition and removal of different forms of DIN, we calculated the changes in the inorganic N fluxes through the REI compared with the fluxes out of the estuary determined at the ECI (Table 5), denoted as flux addition in the unit of t day^{-1} and % of REI fluxes. In many cases, there was a net addition of inorganic N species within the estuary. In the group of AP, there was a small addition of ammonium-N (0.2–3.2 t day^{-1} and 0.8–9.8%), a small addition of nitrite-N (1.8–5.6 t day^{-1} and 45.0–72.6%) and variable fluxes of nitrate-N (− 3.4 to 8.6 t day^{-1} and − 2.5% to 10.0%), while there was a large removal of ammonium-N (1.9–9.4 t day^{-1} and 15.3–57.7%), large addition of nitrite-N (9.2–19.0 t day^{-1} and 142.6–376.3%) and variable nitrate-N (− 5.8 to 3.2 t day^{-1} and − 9.7% to 3.6%) in the RP group (Table 5). The NO_2-N fluxes addition (t day^{-1}) were even higher than the reduced NH_4-N fluxes in the RP group. Moreover, the average NO_2-N fluxes addition

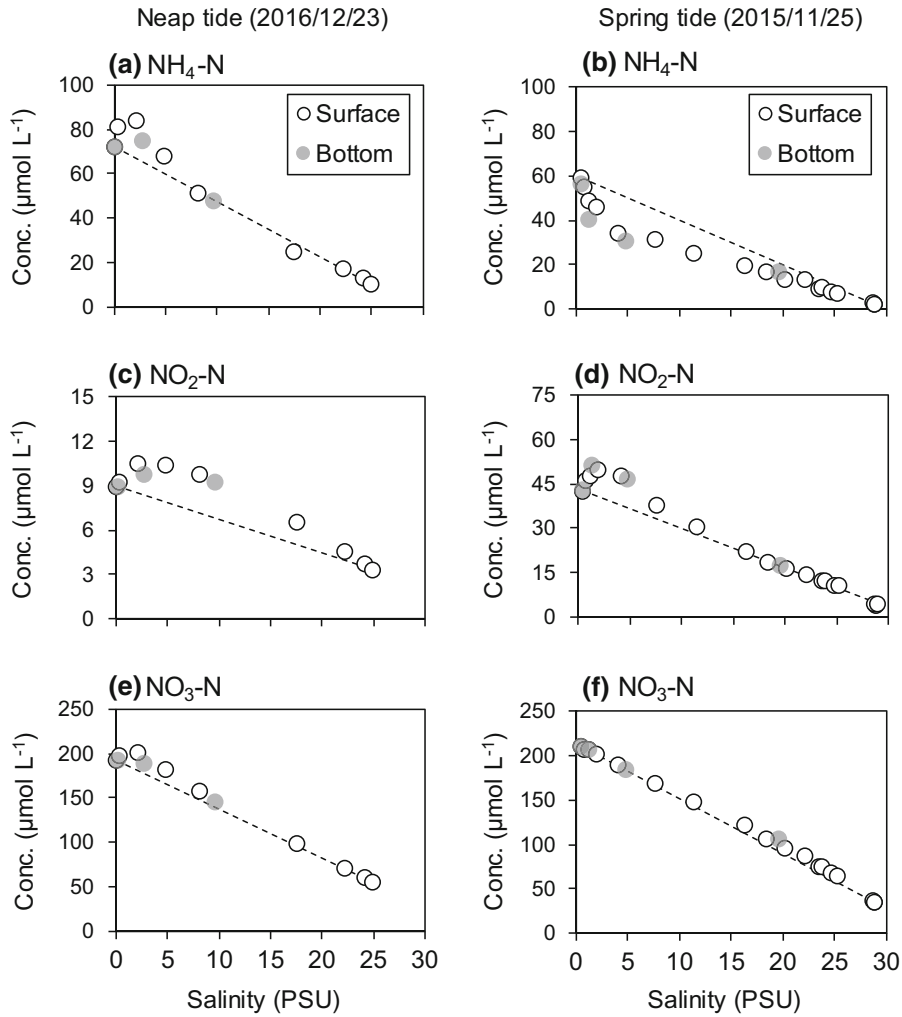

Fig. 5 Dissolved inorganic nitrogen concentrations of surface and bottom water versus salinity in the Jiulong River Estuary on 23rd December 2016 close to a neap tide (in NH_4-N Addition Pattern group) and 25th November 2015 close to a spring tide (in NH_4-N Removal Pattern group). The dashed line is the conservative mixing line between the end-members. NH_4-N Addition Pattern indicates that an ammonium addition pattern was observed in the upper estuary. NH_4-N Removal Pattern indicates that an ammonium removal was observed in the upper estuary. We did not collect bottom samples for nitrogen concentrations during the cruise on 6th May 2015 in Fig. 3, so we chose the cruise on 23rd December 2016 to represent the state of a neap tide

percentage in the RP group was 250.5%, 4.3 times of that in the AP group (57.1%) (Table 5). As for the flood-affected cruise in May 2015, NH_4-N fluxes at the REI was as high as 86.8 t day^{-1} and then increased to 134.8 t day^{-1} at the ECI (Table 5). Meanwhile, DIN fluxes increased by 69.3 t day^{-1}, of which 69.3% was contributed by ammonium-N and 30.7% by nitrate + nitrite (Table 6).

Discussion

Variations of SPM and sediment processes in ETM under different hydrological conditions

According to the definition of "baseflow" and "flood-affected" hydrological conditions in "Auxiliary data collection and data analysis" section, most of the cruises in this study were carried out during baseflow conditions (Fig. 2a). The only exception was in May 2015, which occurred during the first flood in 2015 (Fig. 2a). Here we combine and compare the results during baseflow (NH_4 AP vs. NH_4 RP) and then compare these baseflow conditions, with May 2015 and previous studies describing storm effects through the same estuarine system (JRE) by Chen et al. (2018).

It was found that there was an ETM at all times. Most ETMs during baseflow conditions were located adjacent to the first increase in salinity often around 10 km downstream of the river outlet (Fig. 4), though the exact position depends on the state of the tide as well as the river flow. The magnitude of the ETM, as defined by the maximum SPM, was significantly greater in RP which were found during or close to

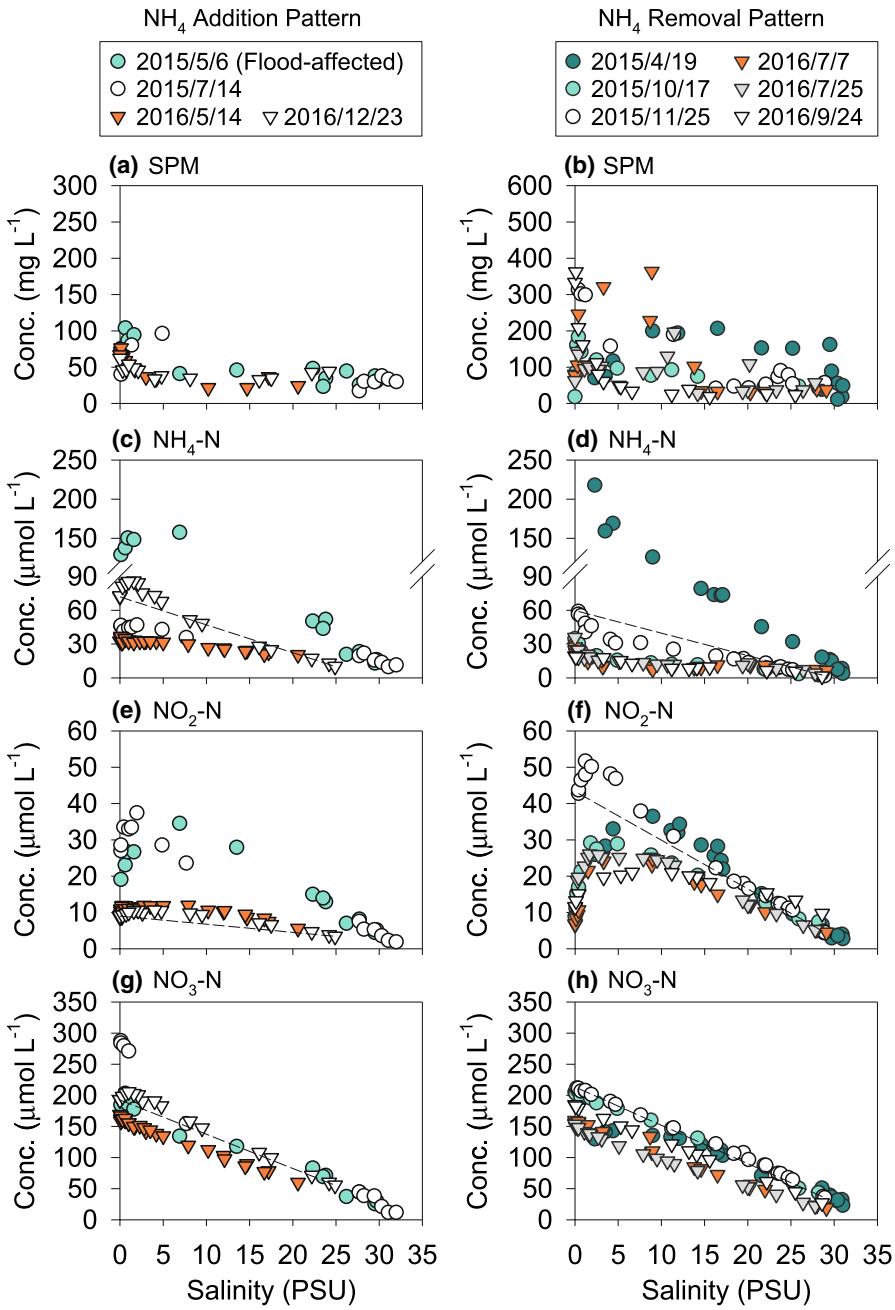

Fig. 6 Suspended particulate matter (SPM) and dissolved inorganic nitrogen concentrations versus salinity in the Jiulong River Estuary in 2015 (circles) and 2016 (triangles). The dashed line is the conservative mixing line between the end-members. The cruises on 23rd December 2016 and 25th November 2015 were chosen as examples for mixing behaviors

spring tides (ranging 142–363 mg L^{-1}, 257 ± 91 mg L^{-1} as mean ± SE) under baseflow conditions, compared to that in AP which were found during or close to neap tides (ranging 62–97 mg L^{-1}, 82 ± 21 mg L^{-1} as mean ± SE) ($p < 0.01$) as shown in Fig. 4. This is consistent with previous studies in macrotidal estuaries, which showed that neap–spring tidal cycles are an important control on

Table 3 Potential ammonium oxidation rates and nitrite oxidation rates during the cruise on 23rd December 2016

Sample stations	Salinity (PSU)	Ammonium oxidation rate (μmol N L^{-1} day^{-1})	Nitrite oxidation rate (μmol N L^{-1} day^{-1})
A8 (low salinity)	2.1	8.78	0.82
JY3 (high salinity)	24.2	0.68	0.04

sedimentological processes (Allen et al. 1980). The ETM, during baseflow conditions, is caused by a saline underflow resuspending fine-grained sediments during the flood tide which is then deposited further downstream during the ebb tide (Schubel 1971). Larger amounts of fine sediments are resuspended and net eroded over a larger area during spring tides, while the opposite occurs during neap tides, where suspended particles tend to be net deposited and then preserved both in the channel and on the banks, although some sediment is eroded, resuspended and deposited during every tidal cycle (Manning and Bass 2006). By contrast, the maximum SPM of ETM was generally higher (223 ± 195 mg L^{-1} as mean ± SE) under flood-affected conditions and was directly proportional to the flood peak discharge, with values as high as 477 mg L^{-1} during an extreme storm in July 2013 (Chen et al. 2018) (Fig. 7a). This was a similar pattern to the ETM in the upper Chesapeake Bay during high flow conditions, where there was a higher sediment load after a large flood event in late January (Sanford et al. 2001). In addition, the location of the ETMs during floods was different from that during baseflow conditions. The locations of the maximum SPM of ETM during storm floods was generally further downstream (Fig. 7b), depending on the magnitude of the peak river discharge (SPM_{max} = 6.63 * $Discharge_{peak}$ + 398.5, R^2 = 0.9626, $p < 0.05$). This flood-enhanced ETM is formed from a combination of the fine-grained sediments brought downstream during the storm flow in the river and its catchment and the sediments resuspended in the upper estuary which was filled with fresh water at that time (Chen et al. 2018). A key difference is that the resuspended sediments during storms, especially the first storm of the year, involves sediments which has been deposited in the estuary for several months and had accumulated the biogeochemical products of the microbial breakdown of organic matter including ammonium in its pore waters and surface sediments. This is particularly intense in a location like the JRE where the water temperature ranges from 18 to 31 °C which is optimal for intensive microbial activities.

Variations of ammonium and other inorganic nitrogen species behavior during different tidal and river flow conditions

Two different states (NH_4 AP and NH_4 RP) of the JRE system were recognized regarding ammonium behavior at low salinities. For the cruises under baseflow conditions, the periods when net ammonium was added to the water column at low salinity (< 2 PSU) was found during or close to neap tides, while the samplings when net ammonium was removed at low salinity (< 2 PSU) was observed during or close to spring tides (Figs. 2b, 6). The average tidal range (± SE) in the AP group (close to neap tides) was 241 (± 19) cm, significantly lower than the value of 316 (± 24) cm in the RP group (close to spring tides) (p = 0.001). Less SPM due to weaker sediment resuspension was found within the first 5–15 km from the river outlet during neap tides compared with the more intense ETM during spring tides which also occurred over a longer reach of the estuary (5–25 km) (Fig. 4). Furthermore, there was a smaller addition of ammonium-N (0.2–3.2 t day^{-1} and 0.8–9.8%) as well as a small addition of nitrite-N (1.8–5.6 t day^{-1} and 45.0–72.6%) and variable changes in nitrate (− 3.4 t day^{-1} to 8.6 t day^{-1} and − 2.5% to 10.0%) in the AP group (Table 5). By contrast, there was a large removal of ammonium-N (1.9–9.4 t day^{-1} and 15.3–57.7%), a larger addition of nitrite-N (9.2–19.0 t day^{-1} and 142.6–376.3%) and a small removal of nitrate (− 5.8 t day^{-1} to 3.2 t day^{-1} and − 9.7% to 3.6%) during periods of RP (Table 5). Ammonium removal and nitrite addition can be connected through a microbially mediated process, nitrification. Nitrite is the product of ammonium oxidation which requires the presence of dissolved oxygen. The vertical structure of salinity and temperature during two cruises showed that the JRE was not

Table 4 Linear regression equations and R^2 in high salinity (> 15 PSU) and comparison of calculated and observed river nitrogen concentrations

Nutrients	NH_4 Addition Pattern					ΔC_0	NH_4 Removal Pattern					ΔC_0
	Cruise dates	Regression equations	R^2	C_0^*	C_0		Cruise dates	Regression equations	R^2	C_0^*	C_0	
Baseflow condition												
NH_4-N	2015/7/14	y = − 1.15x + 49.3	0.97	49.3	46.1	3.2	2015/10/17	y = − 0.53x + 18.4	0.97	18.4	34.7	− 16.3
	2016/5/14	y = − 0.77x + 35.3	0.97	35.3	35.0	0.3	2016/7/7	y = − 0.17x + 11.6	0.95	11.6	24.4	− 12.8
	2016/12/23	y = − 2.79x + 79.0	0.98	79.0	72.0	7.0	2016/7/25	y = − 0.30x + 15.1	0.96	15.1	35.7	− 20.6
							2016/9/24	y = − 0.43x + 16.2	0.95	16.2	19.2	− 3.0
NO_3-N	2015/7/14	y = − 8.87x + 290.4	0.92	290.4	287.7	2.7	2015/10/17	y = − 5.95x + 212.3	0.99	212.3	204.9	7.4
	2016/5/14	y = − 4.77x + 158.2	0.99	158.2	162.3	− 4.1	2016/7/7	y = − 4.48x + 148.1	0.99	148.1	155.4	− 7.3
	2016/12/23	y = − 6.34x + 211.7	0.99	211.7	192.5	19.2	2016/7/25	y = − 4.21x + 138.4	0.99	138.4	153.3	− 14.9
							2016/9/24	y = − 5.32x + 179.8	0.99	179.8	184.6	− 4.8
NO_2-N	2015/7/14	y = − 1.25x + 41.4	0.99	41.4	27.0	14.4	2015/10/17	y = − 0.96x + 33.9	0.99	33.9	9.0	24.9
	2016/5/14	y = − 0.48x + 15.9	0.96	15.9	9.2	6.7	2016/7/7	y = − 0.99x + 32.6	0.99	32.6	6.8	25.8
	2016/12/23	y = − 0.38x + 13.0	0.99	13.0	9.0	4.0	2016/7/25	y = − 1.10x + 35.1	0.99	35.1	11.5	23.6
							2016/9/24	y = − 0.60x + 28.0	0.98	28.0	11.5	16.5
Flood-affected condition												
NH_4-N	2015/5/6	y = − 6.46x + 200.6	0.99	200.6	129.1	71.5						
NO_3-N	2015/5/6	y = − 5.35x + 190.5	0.98	190.5	184.5	6.0						
NO_2-N	2015/5/6	y = − 1.35x + 44.9	0.99	44.9	19.1	25.8						

NH_4-N Addition Pattern indicates that an ammonium addition pattern was observed in the upper estuary. NH_4-N Removal Pattern indicates that an ammonium removal was observed in the upper estuary. The linear regression equations and R^2 in high salinity (> 15 PSU) was obtained using the procedure developed by Officer (1979). x stands for salinity (PSU) and y stands for nitrogen concentration (μmol L^{-1}). This regression line was then extrapolated back to salinity = 0 PSU to get a calculated concentration, C_0^* (μmol L^{-1}). The observed most downriver freshwater concentration was denoted as C_0 (μmol L^{-1}). The cruises on 17th April and 25th November 2015 were excluded in this table because no zero salinity water samples were captured. ΔC_0 (μmol L^{-1}) = $C_0^* - C_0$

Table 5 Dissolved inorganic nitrogen fluxes at REI and ECI

Nutrients	NH_4 Addition Pattern					NH_4 Removal Pattern				
	Cruise dates	REI flux (t day^{-1})	ECI flux (t day^{-1})	Flux addition (t day^{-1})	Flux addition ratio (%)	Cruise dates	REI flux (t day^{-1})	ECI flux (t day^{-1})	Flux addition (t day^{-1})	Flux addition ratio (%)
Baseflow condition										
NH_4-N	2015/7/14	14.8	15.8	1.0	7.0	2015/10/17	14.7	7.8	− 6.9	− 47.0
	2016/5/14	29.5	29.7	0.2	0.8	2016/7/7	18.0	8.6	− 9.4	− 52.4
	2016/12/23	32.3	35.5	3.2	9.8	2016/7/25	13.9	5.9	− 8.0	− 57.7
						2016/9/24	12.2	10.3	− 1.9	− 15.3
NO_3-N	2015/7/14	92.0	92.9	0.9	0.9	2015/10/17	87.0	90.1	3.2	3.6
	2016/5/14	136.9	133.4	− 3.4	− 2.5	2016/7/7	114.7	109.3	− 5.4	− 4.7
	2016/12/23	86.4	95.0	8.6	10.0	2016/7/25	59.7	53.9	− 5.8	− 9.7
						2016/9/24	117.1	114.1	− 3.1	− 2.6
NO_2-N	2015/7/14	8.6	13.2	4.6	53.6	2015/10/17	3.8	14.4	10.6	278.5
	2016/5/14	7.8	13.4	5.6	72.6	2016/7/7	5.1	24.1	19.0	376.3
	2016/12/23	4.0	5.9	1.8	45.0	2016/7/25	4.5	13.7	9.2	204.7
						2016/9/24	7.3	17.8	10.4	142.6
DIN	2015/7/14	115.4	121.9	6.5	5.6	2015/10/17	105.5	112.3	6.8	6.5
	2016/5/14	174.2	176.6	2.5	1.4	2016/7/7	137.7	141.9	4.1	3.0
	2016/12/23	122.7	136.3	13.6	11.1	2016/7/25	78.1	73.5	− 4.6	− 5.9
						2016/9/24	136.6	142.1	5.5	6.4
Flood-affected condition										
NH_4-N	2015/5/6	86.8	134.8	48.0	55.4					
NO_3-N	2015/5/6	124.0	128.0	4.0	3.3					
NO_2-N	2015/5/6	12.8	30.2	17.3	135.4					

NH_4-N Addition Pattern indicates that an ammonium addition pattern was observed in the upper estuary. NH_4-N Removal Pattern indicates that an ammonium removal was observed in the upper estuary. Flux addition (t day^{-1}) = ECI flux − REI flux. Flux addition ratio (%) = (ECI flux − REI flux)/REI flux × 100

REI river–estuary interface, *ECI* estuary–coast interface

strongly stratified during spring tides (top-to-bottom salinity stratification < 0.5 PSU) because of its shallow depth and fast water current, while it showed minor stratification during neap tides particularly in the middle and lower part of the estuary (maximum top-to-bottom salinity stratification > 5 PSU) (Fig. 3). These data shows that the JRE was somewhat stratified similar to the spring–neap cycle of stratification that was found in the York River where it met the Chesapeake Bay, with regularly 3–7 PSU of top-to-bottom stratification around neap tide and less than 1–2 PSU vertical stratification around spring tide in the middle and lower parts of the estuary (Friedrichs 2009; Haas 1977). The salinity stratification can exceed 16 PSU in a typical stratified estuary like the Hudson Estuary (Nepf and Geyer 1996). DO at the bottom was found to be somewhat lower (0.48–1.19 mg L^{-1}) than that at the surface in the low salinity area (< 2 PSU) (Table 2). By contrast, further down the estuary there was higher DO in the bottom water in locations where relatively large vertical salinity difference was found. It is suggested that this was caused by the higher proportion of the sea-end water carrying higher DO (Tables 1, 2). Despite the vertical differences of DO in the estuary, DO concentrations in the water column in the JRE were always above the hypoxia threshold. With abundant ammonium and sufficient oxygen, the water column of the JRE is an ideal place for nitrification. Nitrification rate was high (8.78 μmol N L^{-1} day^{-1} of ammonium oxidation rate and 0.82 μmol N L^{-1} day^{-1} of nitrite oxidation rate) in the brackish water of the JRE during the winter cruise in December 2016 (Table 3), which could be even higher in summer as seasonal variations of nitrification rates have been found in the upstream portion of the Pearl River Estuary (Dai et al. 2008). Moreover, two-step nitrification has shown that ammonium oxidation rates were about 10–20 times faster than nitrite oxidation rates (Table 3). This implies that while ammonium is removed from the water column, nitrite will accumulate through nitrification since it has not yet oxidized to nitrate. This was observed as the peak of nitrite was further downstream than the first reduction of ammonium during both periods of AP and RP (Fig. 6).

Nitrite can also be an intermediate of denitrification, the contribution of which mainly depends on the oxygen status of the water column. Denitrification mainly occurs in the anaerobic sediments resulting in a rapid turnover of nitrate and nitrite (Dong et al. 2002). Typically nitrite is undetectable or only composes a small proportion of DIN in sediment pore waters (Conley et al. 1997). As for the denitrification in the water column, it is usually found in an ETM with fluid mud, in which the SPM concentration exceeds 100 g L^{-1} and the water becomes anoxic (Abril et al. 2000). The SPM in the water column of the JRE was mostly less than 1 g L^{-1} (Figs. 4, 7) (Guo and Jiang 2010). Moreover, no anoxic zone was found in the water column of the JRE although anoxic microniches were possible. If denitrification was a major process in the JRE, it would be expected to have a clear net loss of nitrate flux through the estuary (Table 5). This was not typically observed. Wu et al. (2013) observed an excess dissolved N_2 (an end product of denitrification and anammox) in the JRE. We speculate that coupled nitrification–denitrification may occur under some circumstances close to the sediment–water interface. The variable nitrate-N flux ($-$ 5.8 t day^{-1} to 8.6 t day^{-1}; Table 5) requires further investigation, as it suggests some as a yet undefined balance between sediment denitrification (and other processes causing the removal of nitrate) and nitrification.

It is potentially possible that ammonium assimilation by phytoplankton might contribute to the removal of ammonium in the JRE, especially during spring and summer when one would normally expect higher primary production (York et al. 2007). No measurements of in situ primary productivity were made during this study. However, the light limitation caused by high turbidity in the upper estuary typically limits the growth of phytoplankton and the assimilation rates of ammonium as shown in other research (Irigoien and Castel 1997; Middelburg and Nieuwenhuize 2000), implying assimilation is unlikely to be a major contributor to ammonium removal in the upper estuary with ETM.

Variations of the concentration of SPM in the water column impacted on the ammonium removal processes. In the NH_4 RP group with higher average SPM in the ETM, there was greater ammonium-N removal and stronger nitrite addition compared with NH_4 AP group (Fig. 6; Tables 4, 5). The NO_2-N flux addition (%) was positively correlated with the maximum SPM ($R^2 = 0.88$, $p < 0.01$) (Fig. 8a). Furthermore, the NO_2-N offset was also positively correlated with SPM (Fig. 8c). This implies that stronger removal processes

Table 6 Flux addition of different inorganic nitrogen species and its contributions to the DIN flux addition under flood-affected conditions. Data in May 2014 and July 2014 were from Chen et al. (2018)

Cruise dates	Flux addition (t day^{-1})			Contribution to the DIN flux addition (%)	
	NO_2-N + NO_3-N	NH_4-N	DIN	NO_2-N + NO_3-N	NH_4-N
2015/5/6	21.3	48.0	69.3	30.7	69.3
2014/5/24	148.1	25.5	173.6	85.3	14.7
2014/7/26	2.8	13.3	16.1	17.3	82.7

Flux addition (t day^{-1}) = ECI flux − REI flux

REI river–estuary interface, *ECI* estuary–coast interface

(mostly nitrification) occurred with higher SPM. Particles and microbes can be connected in two ways. Microbes, such as nitrifiers can be introduced from the surface sediment during the resuspension. AOA and AOB are abundant in the uppermost aerobic layer of the sediments, which results in active nitrification in the sediments (Beman and Francis 2006; Luo et al. 2014). In addition, the nitrification rate was positively correlated with the diversity and abundance of nitrifiers at the water–sediment interface (Luo et al. 2014). At the same time, higher SPM can provide more available particulate surfaces for microbes such as nitrifying bacteria or archaea to attach to and multiply in the water column. It has been shown that near bottom waters or fluid muds with higher SPM have higher attached ammonium oxidizing bacterial cells than the surface water (Abril et al. 2000; Stehr et al. 1995).

Ammonium can also be removed by adsorption onto particles. Increasing SPM could raise the capacity for ammonium adsorbed onto particles (Hou et al. 2003; Shen et al. 1997). It was shown that the SPM increased by 2.3–9.9 times (Fig. 4) in the RP group, implying ammonium adsorption onto particles could be important. However, since the resuspended sediment particles generally come from sediments attached with high concentrations of ammonium, it is more likely that ammonium was supplied to the water column by desorption from the particles particularly during the mixing of fresh and saline water (Rysgaard et al. 1999). These findings suggest that nitrification was the major process transforming inorganic N species in the JRE during baseflow regimes and that a large fraction of such nitrification occurred at the ETM. More detailed research on the contribution of ammonium from the sediments and the process of nitrification in the ETM of the JRE are needed in the future.

Ammonification is an important process adding ammonium in the estuary systems and is very active in sediments with abundant organic matter like a salt marsh or bed sediments (Li et al. 2015; Sumi and Koike 1990). Abundant ammonium can be regenerated from ammonification of organic matter in the upper 10–20 cm of the sediment column (Callender and Hammond 1982; Fisher et al. 1982). In addition, DNRA could also make a small contribution to the accumulation of ammonium in anaerobic sediments (An and Gardner 2002; Gardner et al. 2006). High ammonium concentrations in pore water were observed in the upper JRE, ranging from 118–4520 μmol L^{-1} during a summer cruise to 38–1220 μmol L^{-1} during a winter cruise in 2014, which indicated ammonium was the dominant inorganic nitrogen species (Hong et al. 2017). Release of ammonium from sediments has been examined by lab sediment core incubations in lakes, reservoirs and estuaries (Morin and Morse 1999; Porter et al. 2010; Reddy et al. 1996), which support the addition of ammonium in the lower salinity area after the increase of SPM (Fig. 6), caused by sediment resuspension and desorption. Ammonium-rich pore water in the sediments is likely to be a major source for DIN addition into the estuarine water column. The amount of ammonium released will be a function of the ammonium built up by ammonification and the amount of sediments resuspended.

It is possible by making some simple assumptions to estimate the magnitude of net ammonium supplied to the estuarine water column. 15.3–57.7% of the ammonium-N supplied at the REI was removed in the RP group under baseflow, while there was a small addition (0.8–9.8%) of ammonium added in the

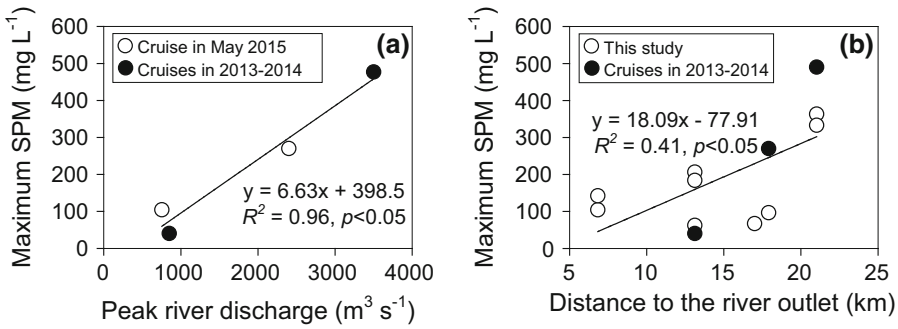

Fig. 7 The relationship between the maximum suspended particular matter (SPM) in the estuarine turbidity maximum and **a** peak river discharge during flood-affected periods and **b** its location under all hydrological conditions. The river outlet is site A3 (refer to Fig. 1). Black circles are from flood-affected cruises in 2013–2014 in Chen et al. (2018)

estuary in the AP group (Table 5). The largest net change was nitrite in which there was a 142.6–376.3% increase within the estuary in the RP group under baseflow, and a smaller but still not inconsiderable increase of 45.0–72.6% in the AP group (Table 5). If we assume that all the NO_2-N addition was converted from ammonium by nitrification and neglect the minor amount of nitrite oxidation, then, the sum of NO_2-N flux addition and NH_4-N flux addition provides an estimate of the total NH_4-N fluxes (denoted as calculated NH_4-N flux addition) into the water column from all addition processes within the estuary. The calculated NH_4-N flux addition (t day^{-1}) ranged from 5.0 to 5.7 t day^{-1} in the AP group and 1.2–9.6 t day^{-1} in the RP group. The percentage of calculated NH_4-N added flux after the ETM to NH_4-N flux at the REI was in proportion to the maximum SPM in the ETM (Fig. 8b). The NH_4-N offset in the AP group was also positively correlated with SPM (Fig. 8d). Moreover, we compared the calculated added NH_4-N flux in areal rates (based on the open water area of the JRE) and the estimated NH_4-N flux rates from sediments in the literature. The added NH_4-N flux in areal rates ranged from 261 to 683 mmol m^{-2} day^{-1} under baseflow in the present study, which is within the range of 1.7–870 mmol m^{-2} day^{-1} of NH_4-N benthic fluxes in the JRE (Hong et al. 2017). It is likely that this addition was mostly from the sediment pore waters and sediment desorption when resuspended into the water column.

Comparison of the DIN export fluxes under baseflow and flood-affected conditions

In this study we have found that although there are differences in the flux addition of N species between NH_4 AP and NH_4 RP states (Tables 4, 5), the DIN flux addition out of the estuary into the coastal zone was comparatively small (from − 4.6 to 13.6 t day^{-1} and − 5.9 to 11.1% under baseflow conditions), which contrasts with the added fluxes during floods or storms, occurring regularly in this region during the summer wet season, when the fluxes of DIN into the estuary through the REI were 16.1–173.6 t day^{-1} (Fig. 9). This was consistent with some other researches. For example, DIN fluxes were increased by 7.2–21.5% under the influence of two typhoon events in the upper Minjiang Estuary and increased by 53.0% under a severe tropical storm in the Yangtze Estuary, compared to that of pre-typhoon (Wang et al. 2016a, b). The increased flux of N species into the estuary was due to the mobilization of both natural and particularly anthropogenic N species in the river catchment, mainly derived from fertilizer, manure and sewage (Yu et al. 2015). Previous work has shown that during storms, high levels of anthropogenic mainly agricultural DIN was flushed into the rivers from the land surface and upper layers of the soil (Chen and Hong 2011). However, it was also found that there was a major increase in the DIN flux addition within the estuary especially for the first flood of the year e.g. May 2014 (173.6 t day^{-1}) and May 2015 (69.3 t day^{-1}) (Table 6). The flux addition of DIN from the storm of July 2014 was lower (16.1 t day^{-1}) because it was a relatively small storm and it was not

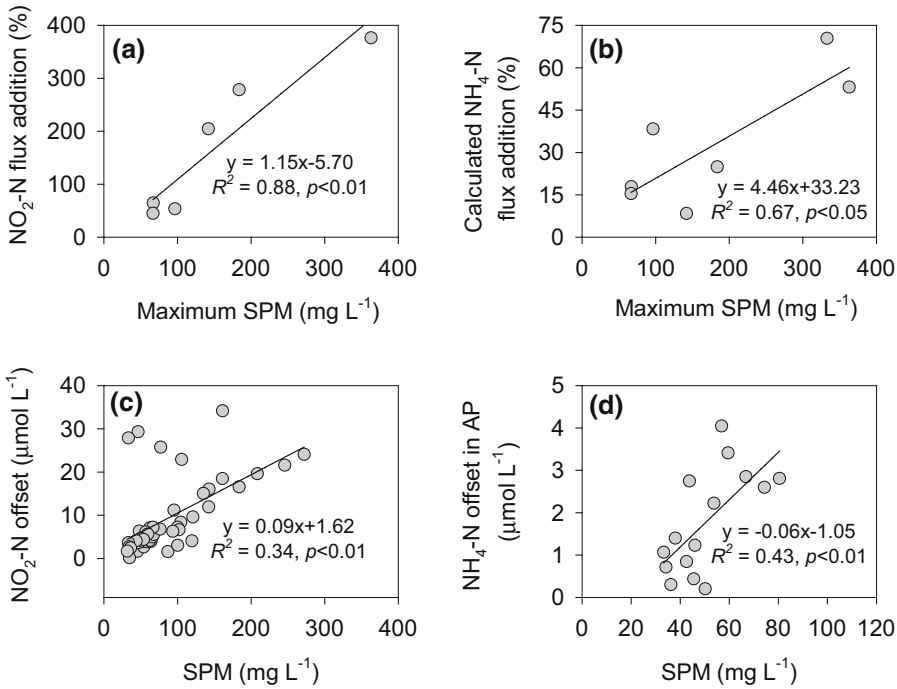

Fig. 8 **a** The relationship between NO_2-N flux addition ((ECI flux − REI flux) × 100)/REI flux) and the maximum suspended particulate matter (SPM) under baseflow conditions. REI represents the river–estuary interface, ECI represents the estuary–coast interface. **b** The relationship between calculated NH_4-N flux addition and the maximum SPM under baseflow conditions. The calculated NH_4-N flux addition = (NH_4-N + NO_2-N added flux) × 100/REI NH_4-N flux. This calculation assumes that all the NO_2-N addition after the estuarine turbidity maximum was contributed by nitrification. REI represents the river–estuary interface. **c** The relationship between NO_2-N offset and SPM. **d** The relationship between NH_4-N offset and SPM in NH_4-N Addition Pattern group (AP). NH_4-N Addition Pattern indicates that an ammonium addition pattern was observed in the upper estuary

the first storm of the year (Chen et al. 2018). This means that there was a major source of DIN within the estuary itself that was mobilized during storms, particularly during the first major flood of the year, compared with the small net export during baseflow (Table 5; Fig. 9). The extra nutrients exported during floods cannot be from riverine DIN temporarily stored in the estuary by adsorption or other such processes during baseflow and released during storms. It must come from a different source.

The most likely source of the additional DIN flux between the REI and the ECI is the breakdown of particulate organic nitrogen (PON). This PON is likely to have accumulated in the sediments in those areas of the upper estuary, where sediments were not resuspended during normal tidal flows. Floods with larger river discharge usually cause a deeper and larger scale scour of estuarine bed sediments from the main channel and sediments from the banks during major storms including the flushing out of adjacent salt marsh deposits (Wengrove et al. 2015). There were 13.3–25.5 t day^{-1} of NH_4-N added fluxes into the estuary during two storms in the JRE in 2014 (Table 6), much higher than the 0.2–3.2 t day^{-1} (0.8–9.8%) of NH_4-N added fluxes under baseflow conditions (Table 5). This sediment accumulates N species in the pore waters both as ammonium produced by microbial decay and as nitrate produced by in situ nitrification (Fisher et al. 1982). During major storms, especially the first storm of the year, this DIN was flushed out into the overlying water and exported as 'new' DIN downstream. However, the observed increase of DIN fluxes during storm flows was not shared equally between N species (Table 6). Major increases were found in ammonium (48.0 t day^{-1}) and a small increase in nitrate + nitrite (21.3 t day^{-1}) in May 2015, while for the major storm on May 2014, the major increase in N exported was

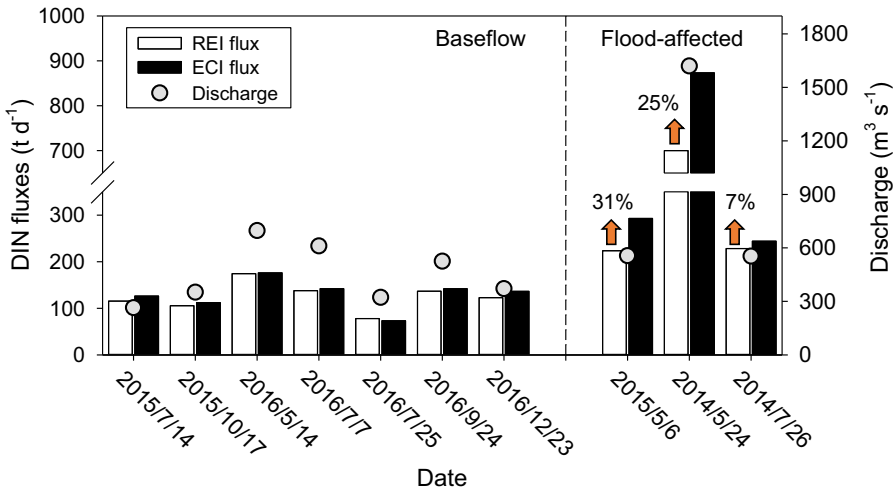

Fig. 9 Dissolved inorganic nitrogen (DIN) fluxes across the river–estuary interface (REI) and across the estuary–coastal interface (ECI). Up arrow and percentage number show increasing proportion from REI flux to ECI flux. Data in May 2014 and July 2014 were adapted from Chen et al. (2018)

mostly as nitrate + nitrite (148.1 t day^{-1}) with 25.5 t day^{-1} of ammonium-N. Further work is required on a series of storms to determine the balance of processes involved in this short-term flushing out of N species from the estuary.

Overall, under flood-affected conditions, the estuary is a source of 'new' DIN which is exported to the coastal areas. This DIN is bioavailable for uptake by phytoplankton within the lower reaches of the estuary and bay. It has been shown that there is an increase phytoplankton about 2 weeks after major storms in the JRE, as soon as the light-suppressing particulate matter has dropped out of the water column (Chen et al. 2018).

We summarized our major findings in the conceptual model in Fig. 10. The neap–spring tidal cycle of the estuary resulted in changes in the pattern of non-conservative behaviour of ammonium and other inorganic N species along the estuary under baseflow conditions. There was net ammonium addition during neap tides and net removal during spring tides. This control was related principally to the magnitude of the sediments resuspended into the water column. There were larger N fluxes during flood-affected conditions, which were caused by a combination of the larger N runoff from the watershed and addition processes within the estuary caused by resuspension of sediments which had been brought down and deposited during previous relatively low flow conditions. The resuspended sediments were particularly rich in organic N breakdown products. This resulted in a considerable increase in the net nutrient supply through the river–estuary system and was potentially likely to stimulate the coastal productivity. Understanding more details on how bioavailable inorganic N species are transported and transformed in hydrological dynamic estuaries is an important issue for eutrophication controls in the estuary and the adjacent coastal zone in the future.

Conclusions

ETM in the JRE varied with the hydrological dynamics of the estuary. During baseflow, there were more intense ETMs during spring tides than neap tides, since the spring tides tend to cause stronger net sediment resuspension than the neap tides. Under flood-affected conditions, a different ETM was present. It has a higher maximum SPM involving sediments brought down by the river augmented by additional sediments resuspended in the upper estuary. Storm flow, especially the first storm of the year, resulted in the resuspension of sediment, which had been deposited during baseflow conditions over several months before the floods in the estuary.

Nitrification is likely one of the most important transformation processes in the water column of the

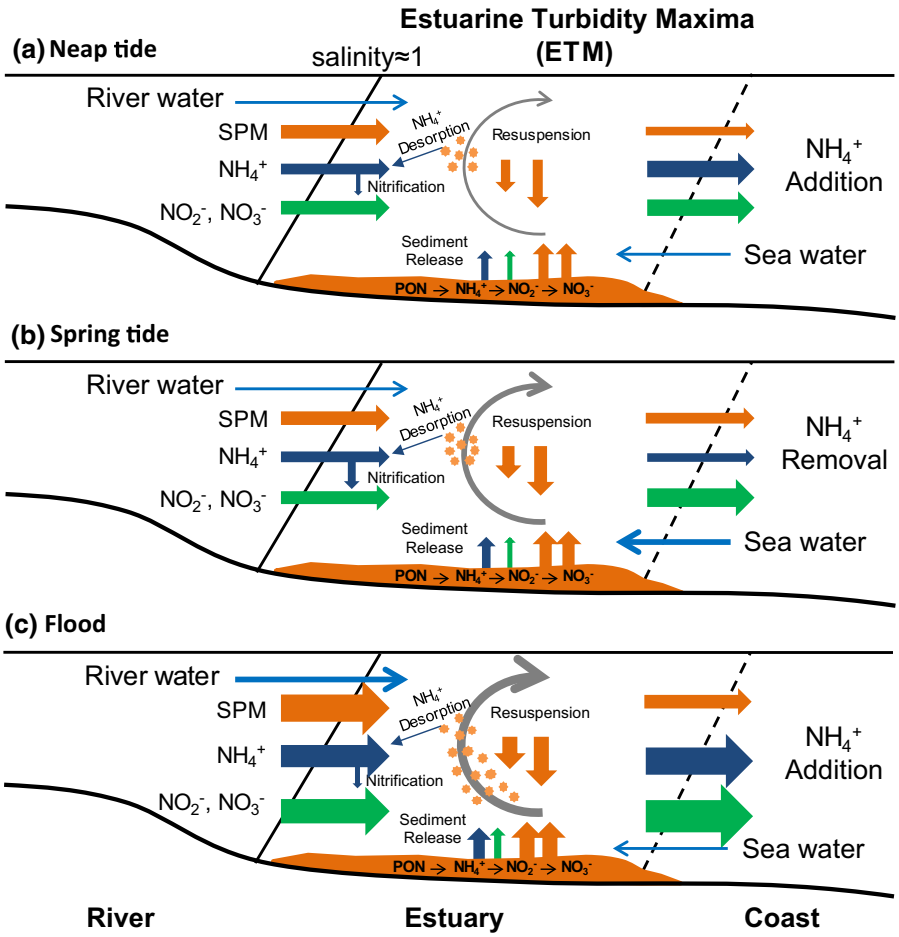

Fig. 10 A conceptual model of ammonium and other inorganic nitrogen biogeochemical processes and fluxes through a subtropical macro-tidal estuary under baseflow (neap tide vs. spring tide) and flood-affected conditions. The wider arrows indicate larger fluxes

turbid part of the JRE, causing much of the removal of ammonium and the addition of nitrite. It is more intense during spring tides because of higher amounts of SPM carrying nitrifying bacteria, although higher amounts of ammonium are resuspended into the oxic water column within the ETM, compared to the situation during neap tides under baseflow conditions. An important source of ammonium to the water column is from resuspended sediments and their pore waters. In general, neap tide tends to exhibit NH_4-N AP while spring tide tends to show NH_4-N removal pattern.

Compared with baseflow conditions, there is more additional DIN exported from the estuary to the coastal areas under flood-affected conditions, in particular during the first flood of the year. This pulse of bioavailable DIN after major floods increases the risk for excess phytoplankton growth in the coastal water areas.

As shown in the conceptual model in Fig. 10, the neap–spring tidal cycle of the estuary resulted in systematic changes in the pattern of the non-conservative behaviours of ammonium and other inorganic nitrogen along the estuary under baseflow conditions, by controlling the magnitude of the sediments. During flood-affected conditions, there were larger N fluxes, which were induced by the larger N runoff from the watershed and stronger addition processes within the estuary from resuspended. This increased nutrient supply from the river catchment and from processes in the estuary are likely to stimulate additional coastal productivity.

Acknowledgements This study was supported by the National Natural Science Foundation of China (Nos. 41676098, 41376082), and Fundamental Research Funds for the Central Universities (Nos. 20720160120, 20720180119). We thank CEES for funding the cruises and Shuiying Huang and Jiezhong Wu for their organizational help. We thank the crew and all the students in Xiamen University on R/V Ocean II for their assistance in the cruises. Michael D. Krom wishes to acknowledge the Visiting Professorship at Xiamen University, where part of this work was accomplished. The authors would like to thank the very detailed comments made by two anonymous reviewers which greatly improved the clarity of the text.

References

Abril G, Etcheber H, Le Hir P, Bassoullet P, Boutier B, Frankignoulle M (1999) Oxic/anoxic oscillations and organic carbon mineralization in an estuarine maximum turbidity zone (The Gironde, France). Limnol Oceanogr 44:1304–1315. https://doi.org/10.4319/lo.1999.44.5.1304

Abril G, Riou SA, Etcheber H, Frankignoulle M, de Wit R, Middelburg JJ (2000) Transient, tidal time-scale, nitrogen transformations in an estuarine turbidity maximum—fluid mud system (The Gironde, south-west France). Estuar Coast Shelf Sci 50:703–715. https://doi.org/10.1006/ecss.1999.0598

Allen GP, Salomon JC, Bassoullet P, Du Penhoat Y, de Grandpré C (1980) Effects of tides on mixing and suspended sediment transport in macrotidal estuaries. Sediment Geol 26:69–90. https://doi.org/10.1016/0037-0738(80)90006-8

An S, Gardner WS (2002) Dissimilatory nitrate reduction to ammonium (DNRA) as a nitrogen link, versus denitrification as a sink in a shallow estuary (Laguna Madre/Baffin Bay, Texas). Mar Ecol Prog Ser 237:41–50. http://www.jstor.org/stable/24866302

Bartlett R, Mortimer RJG, Morris K (2008) Anoxic nitrification: evidence from Humber Estuary sediments (UK). Chem Geol 250:29–39. https://doi.org/10.1016/j.chemgeo.2008.02.001

Beman JM, Francis CA (2006) Diversity of ammonia-oxidizing archaea and bacteria in the sediments of a hypernutrified subtropical estuary: Bahia del Tobari, Mexico. Appl Environ Microbiol 72:7767–7777. https://doi.org/10.1128/AEM.00946-06

Bianchi TS (2007) Biogeochemistry of estuaries. Oxford University, Demand, Oxford

Bianchi M, Feliatra F, Tréguer P, Vincendeau M-A, Morvan J (1997) Nitrification rates, ammonium and nitrate distribution in upper layers of the water column and in sediments of the Indian sector of the Southern Ocean. Deep Sea Res II 44:1017–1032. https://doi.org/10.1016/S0967-0645(96)00109-9

Callender E, Hammond DE (1982) Nutrient exchange across the sediment–water interface in the Potomac River Estuary. Estuar Coast Shelf Sci 15:395–413. https://doi.org/10.1016/0272-7714(82)90050-6

Cao W, Hong H, Yue S (2005) Modelling agricultural nitrogen contributions to the Jiulong River Estuary and coastal water. Glob Planet Change 47:111–121. https://doi.org/10.1016/j.gloplacha.2004.10.006

Chen N, Hong H (2011) Nitrogen export by surface runoff from a small agricultural watershed in southeast China: seasonal pattern and primary mechanism. Biogeochemistry 106:311–321. https://doi.org/10.1007/s10533-010-9514-6

Chen S, Ruan W, Zhang L (1985) Chemical characteristics of nutrient elements in the Jiulong Estuary and the calculation of its flux. Trop Oceanol 4:16–24

Chen G, Chen B, Yu D, Tam NFY, Ye Y, Chen S (2016) Soil greenhouse gas emissions reduce the contribution of mangrove plants to the atmospheric cooling effect. Environ Res Lett 11:124019

Chen N, Krom MD, Wu Y, Yu D, Hong H (2018) Storm induced estuarine turbidity maxima and controls on nutrient fluxes across river–estuary–coast continuum. Sci Total Environ 628–629:1108–1120. https://doi.org/10.1016/j.scitotenv.2018.02.060

Conley DJ, Stockenberg A, Carman R, Johnstone RW, Rahm L, Wulff F (1997) Sediment–water nutrient fluxes in the Gulf of Finland, Baltic Sea. Estuar Coast Shelf Sci 45:591–598. https://doi.org/10.1006/ecss.1997.0246

Crowe SA, Canfield DE, Mucci A, Sundby B, Maranger R (2012) Anammox, denitrification and fixed-nitrogen removal in sediments from the Lower St. Lawrence Estuary. Biogeosciences 9:4309. https://doi.org/10.5194/bg-9-4309-2012

Dai M, Wang L, Guo X, Zhai W, Li Q, He B, Kao S-J (2008) Nitrification and inorganic nitrogen distribution in a large perturbed river/estuarine system: the Pearl River Estuary, China. Biogeosciences 5:1227–1244

Damashek J, Casciotti K, Francis C (2016) Variable nitrification rates across environmental gradients in turbid, nutrient-rich estuary waters of San Francisco Bay. Estuaries Coasts 39:1050–1071. https://doi.org/10.1007/s12237-016-0071-7

de Wilde HPJ, de Bie MJM (2000) Nitrous oxide in the Schelde Estuary: production by nitrification and emission to the atmosphere. Mar Chem 69:203–216. https://doi.org/10.1016/S0304-4203(99)00106-1

Dong LF, Nedwell DB, Underwood GJ, Thornton DC, Rusmana I (2002) Nitrous oxide formation in the Colne Estuary, England: the central role of nitrite. Appl Environ Microbiol 68:1240–1249. https://doi.org/10.1128/AEM.68.3.1240-1249.2002

Erler DV et al (2014) Nitrogen transformations within a tropical subterranean estuary. Mar Chem 164:38–47. https://doi.org/10.1016/j.marchem.2014.05.008

Falco S, Nienchesk L, Rodilla M, Romero I, del Río JG, Sierra JP, Mösso C (2010) Nutrient flux and budget in the Ebro Estuary. Estuar Coast Shelf Sci 87:92–102. https://doi.org/10.1016/j.ecss.2009.12.020

Fichez R, Jickells T, Edmunds H (1992) Algal blooms in high turbidity, a result of the conflicting consequences of turbulence on nutrient cycling in a shallow water estuary. Estuar Coast Shelf Sci 35:577–592. https://doi.org/10.1016/S0272-7714(05)80040-X

Fisher TR, Carlson PR, Barber RT (1982) Sediment nutrient regeneration in three North Carolina estuaries. Estuar

Coast Shelf Sci 14:101–116. https://doi.org/10.1016/S0302-3524(82)80069-8

Friedrichs CT (2009) York River physical oceanography and sediment transport. J Coast Res Special Issue 57:17–22. https://doi.org/10.2112/1551-5036-57.sp1.17

Gao X, Chen N, Yu D, Wu Y, Huang B (2018) Hydrological controls on nitrogen (ammonium versus nitrate) fluxes from river to coast in a subtropical region: observation and modeling. J Environ Manag 213:382–391. https://doi.org/10.1016/j.jenvman.2018.02.051

Gardner WS, McCarthy MJ, An S, Sobolev D, Sell KS, Brock D (2006) Nitrogen fixation and dissimilatory nitrate reduction to ammonium (DNRA) support nitrogen dynamics in Texas estuaries. Limnol Oceanogr 51:558–568. https://doi.org/10.4319/lo.2006.51.1_part_2.0558

Garnier J, Billen G, Némery J, Sebilo M (2010) Transformations of nutrients (N, P, Si) in the turbidity maximum zone of the Seine Estuary and export to the sea. Estuar Coast Shelf Sci 90:129–141. https://doi.org/10.1016/j.ecss.2010.07.012

Grabemann I, Uncles RJ, Krause G, Stephens JA (1997) Behaviour of turbidity maxima in the Tamar (U.K.) and Weser (F.R.G.) Estuaries. Estuar Coast Shelf Sci 45:235–246. https://doi.org/10.1006/ecss.1996.0178

Guo M, Jiang Y (2010) Distribution of suspended sediment and erosion simulation of the Jiulong River Estuary during a flood process. J Xiamen Univ (Nat Sci) 49:688–693

Guo W, Xia E, Han Y, Wu F, Li M, Wu Y (2005) Fluorescent characteristics of colored dissolved organic matter (CDOM) in the Jiulong River Estuary. Oceanol Limnol Sin 36:356

Haas LW (1977) The effect of the spring-neap tidal cycle on the vertical salinity structure of the James, York and Rappahannock Rivers, Virginia, USA. Estuar Coast Mar Sci 5:485–496. https://doi.org/10.1016/0302-3524(77)90096-2

Herman PM, Heip CH (1999) Biogeochemistry of the MAximum TURbidity Zone of Estuaries (MATURE): some conclusions. J Mar Syst 22:89–104. https://doi.org/10.1016/S0924-7963(99)00034-2

Hong H, Lin J (1990) Preliminary study on the distribution of nutrients, organic matter, trace metals in sea surface microlayer in Xiamen Bay and Jiulong Estuary. Acta Oceanol Sin 9:81–90

Hong Q, Cai P, Shi X, Li Q, Wang G (2017) Solute transport into the Jiulong River Estuary via pore water exchange and submarine groundwater discharge: new insights from $^{224}Ra/^{228}Th$ disequilibrium. Geochim Cosmochim Acta 198:338–359. https://doi.org/10.1016/j.gca.2016.11.002

Hou LJ, Liu M, Jiang HY, Xu SY, Ou DN, Liu QM, Zhang BL (2003) Ammonium adsorption by tidal flat surface sediments from the Yangtze Estuary. Environ Geol 45:72–78. https://doi.org/10.1007/s00254-003-0858-2

Irigoien X, Castel J (1997) Light limitation and distribution of chlorophyll pigments in a highly turbid estuary: the Gironde (SW France). Estuar Coast Shelf Sci 44:507–517. https://doi.org/10.1006/ecss.1996.0132

Jiang YW, Wai OWH (2005) Drying–wetting approach for 3D finite element sigma coordinate model for estuaries with large tidal flats. Adv Water Resour 28:779–792. https://doi.org/10.1016/j.advwatres.2005.02.004

Li F, Wu Y, Wang L (1964) Physico-chemical processes of silicates in the estuarial region I. Oceanol Limnol Sin 6:311–321

Li X, Hou L, Liu M, Lin X, Li Y, Li S (2015) Primary effects of extracellular enzyme activity and microbial community on carbon and nitrogen mineralization in estuarine and tidal wetlands. Appl Microbiol Biotechnol 99:2895–2909. https://doi.org/10.1007/s00253-014-6187-4

Luo Z, Qiu Z, Wei Q, Du Laing G, Zhao Y, Yan C (2014) Dynamics of ammonia-oxidizing archaea and bacteria in relation to nitrification along simulated dissolved oxygen gradient in sediment–water interface of the Jiulong River estuarine wetland, China. Environ Earth Sci 72:2225–2237. https://doi.org/10.1007/s12665-014-3128-6

Manning AJ, Bass SJ (2006) Variability in cohesive sediment settling fluxes: observations under different estuarine tidal conditions. Mar Geol 235:177–192. https://doi.org/10.1016/j.margeo.2006.10.013

Mayorga E et al (2010) Global nutrient export from WaterSheds 2 (NEWS 2): model development and implementation. Environ Model Softw 25:837–853. https://doi.org/10.1016/j.envsoft.2010.01.007

Middelburg JJ, Nieuwenhuize J (2000) Uptake of dissolved inorganic nitrogen in turbid, tidal estuaries. Mar Ecol Prog Ser 192:79–88. https://doi.org/10.3354/meps192079

Middelburg JJ, Klaver G, Nieuwenhuize J, Wielemaker A, de Hass W, Vlug T, van der Nat JF (1996) Organic matter mineralization in intertidal sediments along an estuarine gradient. Mar Ecol Prog Ser 132:157–168. http://www.jstor.org/stable/24856023

Morin J, Morse JW (1999) Ammonium release from resuspended sediments in the Laguna Madre Estuary. Mar Chem 65:97–110. https://doi.org/10.1016/S0304-4203(99)00013-4

Nathan R, McMahon T (1990) Evaluation of automated techniques for base flow and recession analyses. Water Resour Res 26:1465–1473. https://doi.org/10.1029/WR026i007p01465

Nepf H, Geyer W (1996) Intratidal variations in stratification and mixing in the Hudson Estuary. J Geophys Res Oceans 101:12079–12086. https://doi-org.ezproxy.lib.uconn.edu/10.1029/96JC00630

Officer CB (1979) Discussion of the behaviour of nonconservative dissolved constituents in estuaries. Estuar Coast Mar Sci 9:91–94. https://doi.org/10.1016/0302-3524(79)90009-4

Paerl HW (1997) Coastal eutrophication and harmful algal blooms: importance of atmospheric deposition and groundwater as "new" nitrogen and other nutrient sources. Limnol Oceanogr 42:1154–1165. https://doi.org/10.4319/lo.1997.42.5_part_2.1154

Park K, Wang HV, Kim SC, Oh JH (2008) A model study of the estuarine turbidity maximum along the main channel of the upper Chesapeake Bay. Estuaries Coasts 31:115–133. https://doi.org/10.1007/s12237-007-9013-8

Porter ET, Mason RP, Sanford LP (2010) Effect of tidal resuspension on benthic–pelagic coupling in an experimental ecosystem study. Mar Ecol Prog Ser 413:33–53. https://doi.org/10.3354/meps08709

Reddy KR, Fisher MM, Ivanoff D (1996) Resuspension and diffusive flux of nitrogen and phosphorus in a hypereutrophic lake. J Environ Qual 25:363–371. https://doi.org/10.2134/jeq1996.00472425002500020022x

Ren F, Gleason B, Easterling D (2001) A numerical technique for partitioning cyclone tropical precipitation. J Trop Meteorol 3:014

Rysgaard S, Thastum P, Dalsgaard T, Christensen PB, Sloth NP (1999) Effects of salinity on NH_4^+ adsorption capacity, nitrification, and denitrification in Danish estuarine sediments. Estuaries 22:21–30. https://doi.org/10.2307/1352923

Sanford LP, Suttles SE, Halka JP (2001) Reconsidering the physics of the Chesapeake Bay estuarine turbidity maximum. Estuaries 24:655–669. https://doi.org/10.2307/1352874

Schubel J (1971) Tidal variation of the size distribution of suspended sediment at a station in the Chesapeake Bay turbidity maximum. Neth J Sea Res 5:252–266. https://doi.org/10.1016/0077-7579(71)90012-3

Seitzinger S et al (2010) Global river nutrient export: a scenario analysis of past and future trends. Glob Biogeochem Cycles. https://doi.org/10.1029/2009GB003587

Shen S, Tu SI, Kemper WD (1997) Equilibrium and kinetic study of ammonium adsorption and fixation in sodium-treated vermiculite. Soil Sci Soc Am J 61:1611–1618. https://doi.org/10.2136/sssaj1997.03615995006100060011x

Stehr G, Böttcher B, Dittberner P, Rath G, Koops H-P (1995) The ammonia-oxidizing nitrifying population of the River Elbe Estuary. FEMS Microbiol Ecol 17:177–186. https://doi.org/10.1016/0168-6496(95)00022-3

Sumi T, Koike I (1990) Estimation of ammonification and ammonium assimilation in surficial coastal and estuarine sediments. Limnol Oceanogr 35:270–286. https://doi.org/10.4319/lo.1990.35.2.0270

Tobias C, Giblin A, McClelland J, Tucker J, Peterson B (2003) Sediment DIN fluxes and preferential recycling of benthic microalgal nitrogen in a shallow macrotidal estuary. Mar Ecol Prog Ser 257:25–36. http://www.jstor.org/stable/24867000

Vahtera E et al (2007) Internal ecosystem feedbacks enhance nitrogen-fixing cyanobacteria blooms and complicate management in the Baltic Sea. AMBIO J Hum Environ 36:186–194. https://doi.org/10.1579/0044-7447(2007)36%5b186:IEFENC%5d2.0.CO;2

Wang T, Liu G, Gao L, Zhu L, Fu Q, Li D (2016a) Biological and nutrient responses to a typhoon in the Yangtze Estuary and the adjacent sea. J Coast Res 32:323–332. https://doi.org/10.2112/jcoastres-d-15-00006.1

Wang T, Liu G, Zhao S, Zhu L, Gao L, Li D (2016b) Influence of two typhoon events on the content and flux of nutrient and organic carbon in the upper Minjiang Estuary. J Appl Oceanogr 1:38–46

Wengrove ME, Foster DL, Kalnejais LH, Percuoco V, Lippmann TC (2015) Field and laboratory observations of bed stress and associated nutrient release in a tidal estuary. Estuar Coast Shelf Sci 161:11–24. https://doi.org/10.1016/j.ecss.2015.04.005

Whitehead P, Crossman J (2012) Macronutrient cycles and climate change: key science areas and an international perspective. Sci Total Environ 434:13–17. https://doi.org/10.1016/j.scitotenv.2011.08.046

Wu J, Chen N, Hong H, Lu T, Wang L, Chen Z (2013) Direct measurement of dissolved N_2 and denitrification along a subtropical river–estuary gradient, China. Mar Pollut Bull 66:125–134. https://doi.org/10.1016/j.marpolbul.2012.10.020

Yan X, Zhai W, Hong H, Li Y, Guo W, Huang X (2012) Distribution, fluxes and decadal changes of nutrients in the Jiulong River Estuary, Southwest Taiwan Strait. Chin Sci Bull 57:2307. https://doi.org/10.1007/s11434-012-5084-4

Yang Y, Hu M (1996) Biogeochemical research in the Jiulong River Estuary. Chinese Ocean Press, Beijing

York JK, Tomasky G, Valiela I, Repeta DJ (2007) Stable isotopic detection of ammonium and nitrate assimilation by phytoplankton in the Waquoit Bay estuarine system. Limnol Oceanogr 52:144–155. https://doi.org/10.4319/lo.2007.52.1.0144

Yu D, Yan W, Chen N, Peng B, Hong H, Zhuo G (2015) Modeling increased riverine nitrogen export: source tracking and integrated watershed–coast management. Mar Pollut Bull 101:642–652. https://doi.org/10.1016/j.marpolbul.2015.10.035

Zhang Y, Wang W, Huang Z (1999) Salinity fronts and chemical behaviour of nutrient in Jiulongjiang Estuary. Mar Environ Sci 18:1–7